ANALOGUE MODELS OF SALT DYNAMICS AND SEDIMENTARY BASIN EVOLUTION ON PASSIVE MARGINS: IMPLICATIONS FOR OFFSHORE NOVA SCOTIA HYDROCARBON EXPLORATION

Sheila Marie Ballantyne

Submitted in Partial Fulfilment of the Requirements
for the Degree of Bachelor of Sciences, Honours
Department of Earth Sciences
Dalhousie University, Halifax, Nova Scotia
April 24, 2006

Dalhousie University

Department of Earth Sciences
Halifax, Nova Scotia
Canada B3H 3J5
(902) 494-2358
FAX (902) 494-6889

DATE: April 24, 2006

AUTHOR: Julie Bellefleur

TITLE: Analogue Models of Salt and Sedimentary Basin Evolution on Passive Margins: Implications for offshore N.S. Hydrocarbons

Degree: BSc Convocation: May 29 Year: 2006

ABSTRACT

The Scotian Basin, offshore Nova Scotia, is a passive margin made up of Triassic evaporites overlain by several kilometres of carbonates, shales, and deltaic sediments, which were deposited as a basinward prograding wedge. The progradation of sediments caused the basinward migration of salt in the paleoslope area with thin-skinned extension in the overburden. Complex salt structures and stratigraphic relationships exist as a result of dynamic depositional systems, syn-depositional salt mobilization, and brittle faulting of the overburden. The Scotian Shelf has been well explored and has proven to be an economic source of hydrocarbons. The Scotian Slope, however, has provided disappointing exploration results and is still not well understood. Lack of knowledge and technically challenging environments has made deepwater exploration on the Scotian Slope a high risk.

This study applies physical experiments with high resolution Particle Imaging Velocimetry (PIV) optical strain monitoring to simulate gravity-driven deformation in passive margin sedimentary wedges overlying a mobile substratum under varying sedimentation patterns and rates. The spatial and temporal structural evolution as well as the salt-sediment interactions is analyzed. The results of this study can help develop mechanically constrained concepts and templates for the interpretation of geological and geophysical data. This thesis used six experiments which explored stagnation, low sedimentation and high sedimentation rates, on horizontal and tilted bases. The results show that structures are controlled by strain rates, which are controlled by sedimentation patterns and rates.

Key Words: Scotian Basin, thin skinned extension, salt mobilization, analogue modelling

TABLE OF CONTENTS

TABLE OF FIGURES

TABLE OF TABLES

ACKNOWLEDGEMENTS

I would like to thank my thesis supervisors, Djordje Grujic and Juergen Adam, for sharing their expertise in a supportive and patient manner. Much thanks also to Csaba Krezsek for sharing his advice, insights, and use of his figures. Thank you to Gesine Adam for her help throughout this process, particularly in the data preparation. For staying excruciatingly long nights during the experiment procedures, I would like to express appreciation to the above four people, as well as Joyia Chakungal, Riley Gibson, Steve King, and Neil Tobey. This thesis would not have been possible without the incredible work done by the above people. I am also so very grateful to my family and friends, here and afar, whose undying encouragement helped me to work through this process and maintain a sense of humour. To the geology students of Dalhousie University, particularly those whom I shared many a late night in the Life Sciences Centre, thank you for all your support. I would like to acknowledge Patrick Ryall who, as the honours theses coordinator, made time to give useful comments to each Earth Sciences honours student. Finally, I would like to thank PPSC researchers, AIF/ACOA, CFI, and Canadian Superior Energy Inc. research grant program, who made this thesis financially possible.

CHAPTER ONE: INTRODUCTION

1.1 Objectives

The purpose of this study is to expand the understanding of the Scotian Slope, offshore Nova Scotia, Canada, using analogue models. Interest in the hydrocarbon potential of the Scotian Slope, has created much need in better understanding the tectonic and depositional evolution of the area. Salt related basins in the shelf and slope area as well as their deepwater extensions are of particular interest. The geology of the Scotian Margin has been well documented in several papers (e.g. Wade and MacLean, 1990; Shimeld, 2004). Where water depth is less than two hundred metres, good well data exists. However, due to high risks and costs associated with drilling, few exploration wells in water greater than 200 metres exist. A significant amount of recent 2D seismic data is available, upon which much of the geological interpretation of the salt deformation structures and related salt provinces on the Scotian Slope has been based (Shimeld, 2004).

Scaled analogue modelling techniques yield fully quantitative 3D information on the dynamic evolution of a natural geological prototype. In this thesis, scaled analogue models with brittle and ductile materials were used to study the evolution of thin-skinned extensional basins formed at passive margins over a mobile (e.g. salt) substratum. Analysis of the surficial deformation, 2D vertical cross sections, and 3D development using high resolution optical monitoring with Particle Imaging Velocimetry (PIV) gives a comprehensive and quantified account of the structural, kinematic, and dynamic evolution of sedimentary basins. These results can be used in conjunction with subsurface geological and geophysical information from the Scotian Slope. There is great potential

for improvement of geological and seismic interpretations of complex salt related stratigrahic relations and structures through this work.

1.2 Evolution of Extension on Passive Margins with respect to salt tectonics

The physical models completed in this study investigate the geological processes and the control parameters of sedimentary basin evolution at passive margins due to salt mobilization and associated deformation. Basin extension styles at passive margins can be classified in two categories. The first involves the extension of basement and formation of rift basins, and is named 'thick-skinned'. The second style does not involve the basement, only the sedimentary cover, and is named 'thin-skinned'. Models produced in this thesis represent thin-skinned deformation of passive continental margins, and consist of down slope gravitational gliding and sliding of post rift succession above a ductile detachment (e.g. salt). A schematic model of a passive continental margin is shown in Figure 1.1. The salt sediments, deposited during the syn-rift or earliest post-rift stages, are overlain by marine sediments, deposited as post-rift units.

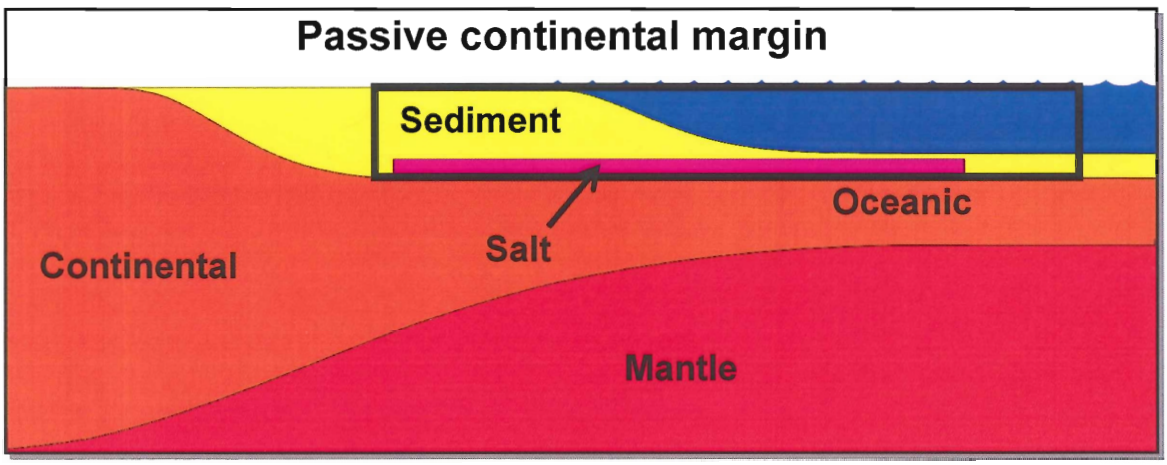

Figure 1.1: Simplified model of passive continental margins (Gemmer et. al., 2002)

Sediment thickness decreases from the continent to the ocean due to sedimentation patterns of the primarily continentally derived material. Thus, a

sedimentary wedge is created, which causes differential loading on the salt substratum. The differential loading creates a pressure gradient and thus gravitational instabilities, causing the sediments to slide and/or glide towards the deep basin over the salt substratum (Vendeville and Jackson, 1991& Gemmer et al., 2004). The cover is thinned as it stretches towards the ocean (or deep basin) which leads to faulting, typically forming narrow, elongate grabens which trend normal to the stretching direction. Such grabens therefore run parallel to the continental margin, observed on passive margins such as the Red Sea and Scotian Slope (Vendeville and Jackson, 1991). The grabens are cored with salt diapirs and salt roller structures, suggesting that the normal faults formed by the extension of overburden act as areas of weaknesses where the diapirs are able to flow upwards (Mart and Ross, 1987; Vendeville and Jackson, 1992a). These structures are discussed in more detail in Chapter Three.

1.3 Geology of the Scotian Basin

The Scotian Basin lays offshore Nova Scotia, Canada. It extends 1200 kilometres, between Georges Bank in the southwest and the Grand Banks in the northeast (Fig. 1.2), with a surface area of ~300,000 km^2. Half of the basin lies on the continental shelf, and the other half on the continental slope at water depths from 200 to 4000 meters (Kidston et. al., 2002). The evolution of the Scotian Slope, which resulted in developing the stratigraphy and structures seen today, began with the rifting of Pangea.

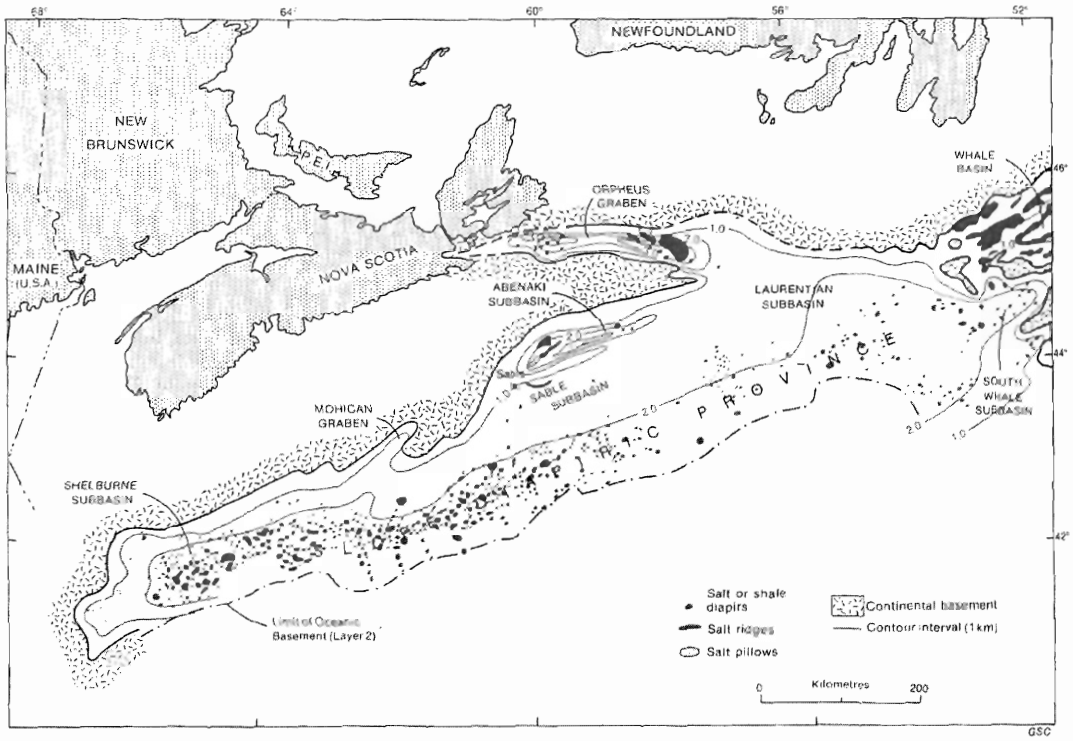

Figure 1.2: Location of the Scotian Basin and Slope diapiric province (Wade & MacLean, 1986)

Rifting was well established by the Late Triassic, forming the beginnings of what is now the Atlantic Ocean (Emery et al., 1984). Throughout the late Triassic and early Jurassic, a series of interconnected grabens and half grabens were developed, creating the Scotian Basin. Isolated graben complexes were also created during this time period in basement lows (Shimeld, 2004). These basins were filled with shallow marine evaporites and sediment units as the Atlantic Ocean continued to open.

The lithostratigraphy of the basin is based on well data (Wade & McLean, 1990; and Shimeld, 2004). The grabens were first filled by the Argo Formation and Eurydice Formation, consisting of evaporates and red continental clastics, respectively (Fig. 1.3).

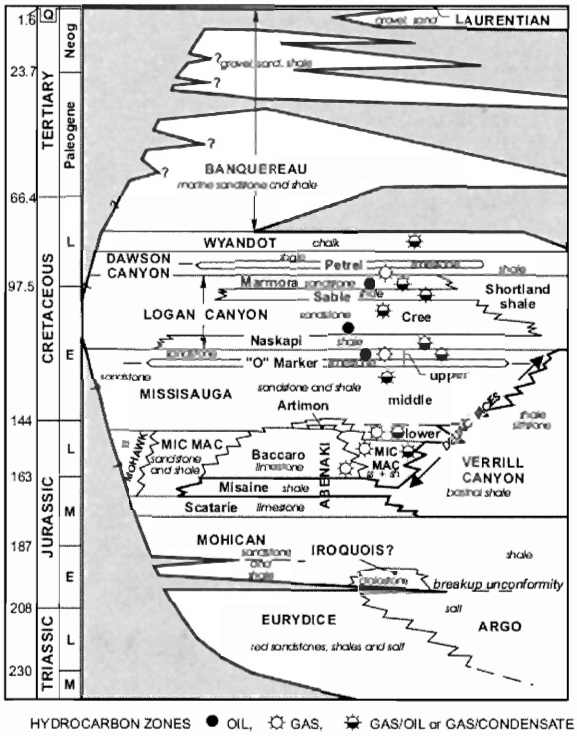

Figure 1.3: Lithostratigraphic chart of the central Scotian Shelf
(Modified from Wade and McLean, 1990 by Shimeld, 2004)

These two Formations are overlain by the Hettangian basalts, followed by an unconformity. The basalts are topped by continental clastics of the Mohican Formation, which overlap some of the basement horsts. Coeval dolomites of the Iroquois Formation mark the paleosurface, and are interpreted as possible sabkha formations (Wade & McLean, 1990). Marine environment developed from the Bajocian until the end of the Jurassic, when the transgressive shale unit and thick shelf carbonates of the Abenaki Formation were deposited (Shimeld, 2004). Alluvial plains and deltas, including the Mohawk and Mic Mac Formations, occurred behind the carbonate bank, while prodelta and deep marine shales of the Verrill Canyon Formation developed beyond the bank (Shimeld, 2004).

During the Early Cretaceous, high sedimentation and marine regression created the thick prodeltaic facies of the Mississauga Formation, later topped by the widespread oolitic limestone unit, marked by the "O" in Figure 1.3.

Coastal plain sediments alternate with transgressive shales in the Logan Canyon Formation, which is overlain by the Dawson Canyon Formation shales and mudstones and the Wyandot Formation marlstone and chalk units. Above these units lies the Banquereau Formation mudstone with regional chalk, sandstone, and conglomerate units (Shimeld, 2004).

In summary, the Scotian Slope has evaporates at its base with an average thickness of 1 km, with an average overlying sediment succession at the shelf-slope break with a thickness of approximately four km. It has been suggested that structures in the basement have an effect on the tectonic development of the basin (Shimeld, 2004). These parameters have been used to develop the models used in this study. The Slope Diapiric Province (Fig. 1.2) has been subdivided by Shimeld into five sub-provinces, defined by their distinctive style of salt deformation and sedimentation history. Sub-province one is dominated by grabens, 8km to 10km thick salt walls, and 15km to 20km seaward salt tongues. A transitional boundary exists between sub-provinces one and two. The tongues diminish in sub-province two, which is dominated by squeezed diapirs and crestal grabens. Sub-province five has extensional features in Cretaceous sections, as well as compressional features in Cretaceous and Neogene strata. In sub-provinces one, two, and five, diapirs have experienced rejuvenation during the Cenozoic. Diapirs here are covered by only Quaternary sediments in some areas. Although there is no well control yet, interpreted seismic strongly suggests the presence of extensive allochthonous salt

canopies in sub-province three. Sub-provinces one, two, and three, have primary salt basins, while the allochthonous salt in sub-province is believed to have been expelled from the Sable subbasin and moved 80km to 100km seaward. There is relatively very little diapirism in sub-province four and has a thick Upper Jurassic syn-kinematic wedge (Shimeld, 2004).

1.4 Kinematic Evolution of Experiments

Each experiment has a sheet of silicone at its base, covered by a layer of sand. The experiments simulate gravity gliding and concomitant brittle deformation of a passive margin sedimentary sequence on top of evaporites. Each experiment simulates the initial build-up stage and later basinward propagation of shelf-slope sedimentary wedge under varying sedimentary patterns and rates. Because the sand cover tapers from the shelf to the deep basin, differential loading is forcing on the underlying silicone to flow towards the area with less pressure (i.e. from the shelf towards the deep basin). The induced pressure gradient and shear stress deforms the viscous fluid silicone (e.g. Turcotte & Schubert, 2002). A channel flow, such as that which occurs in the experiments' silicone, occurs in diverse geological examples, commonly with rigid bounding plates. The plates may also be ductile and allowed to fail (Grujic, in press). In rigid bounding plates models, such as the experiments in this thesis, the simplest characteristic of the 1D velocity field is a hybrid between two end-member components: Couette flow (simple shear) where induced shear across the channel produces uniform vorticity, and Poiseuille flow where the induced pressure gradient produces the highest velocity in the centre and opposite vorticity for the top and bottom of the channel. The sediments overlying the silicone are passively carried towards the deep basin by Couette

flow. Poiseuille flow produces shear traction at the base of the overburden, resulting in the force F_p, which is a function of the ratio between overburden thickness and viscous layer thickness (Grujic, in press). Figure 1.4 shows the forces in a brittle-ductile system, which can be used to predict the style of brittle deformation in the overburden (Lehner, 2000).

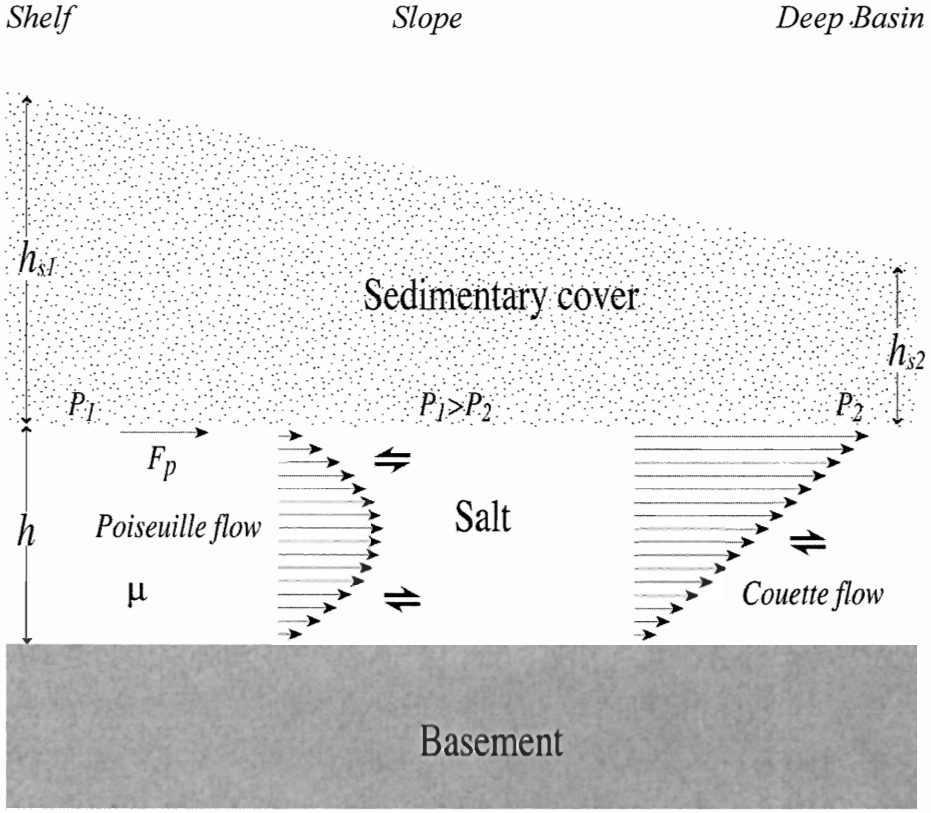

Figure 1.4: Velocity end-members in a viscous layer beneath a brittle-plastic overburden. Differential loading ($p_1>p_2$) is caused by the different sediment thickness ($h_{s1}>h_{s2}$). The Poiseuille flow component is controlled by the magnitude of the pressure difference, the thickness of the viscous layer h and the viscosity m of the weak layer. Displacement of the overburden with respect to the weak viscous layer induces the Couette flow. Poiseuille flow produces shear traction on the base of the overburden resulting in the horizontal force F_p (after Gemmer et al., 2004 and Grujic in press).

The system is stable when:

$$F_1 + F_p = F_2 + F_c \quad (1.1)$$

(Gemmer et al., 2004) where F_1 and F_2 are the horizontal forces in the overburden, F_p is the traction force caused by Poiseuille flow and F_c the force caused by negative traction or Couette flow at the base of the overburden. The silicone is driven basinward by differential loading which causes F_p to increase. If both sides of Equation 1.1 are equal, the system is in equilibrium and there is no flow. When the left side of Equation 1.1 is greater than the right, Couette flow increases and deformation begins. Experiments which are conducted on a tilted base deform according to the same criteria, but because there is a greater height difference created by the tilt there is greater related potential energy due to gravity. Thus, the flow rate is higher because of higher stress and strain rates in tilted models, causing them to deform faster than models on a flat base.

A prominent velocity discontinuity exists at the shelf-slope transition, where the overburden sand sequence is affected by extensional deformation and grabens are initiated (Fig. 1.5). The slope area is passively transported towards the deep basin on top of the mobilized silicone layer. This slope section glides towards the deep basin as a relatively undeformed block (or raft). Simultaneously, the basin area in front of the slope undergoes compressional deformation. New grabens form as the model develops, always initiating at the shelf-slope transition, which propagates depending on sedimentation patterns and rates of the individual experiments.

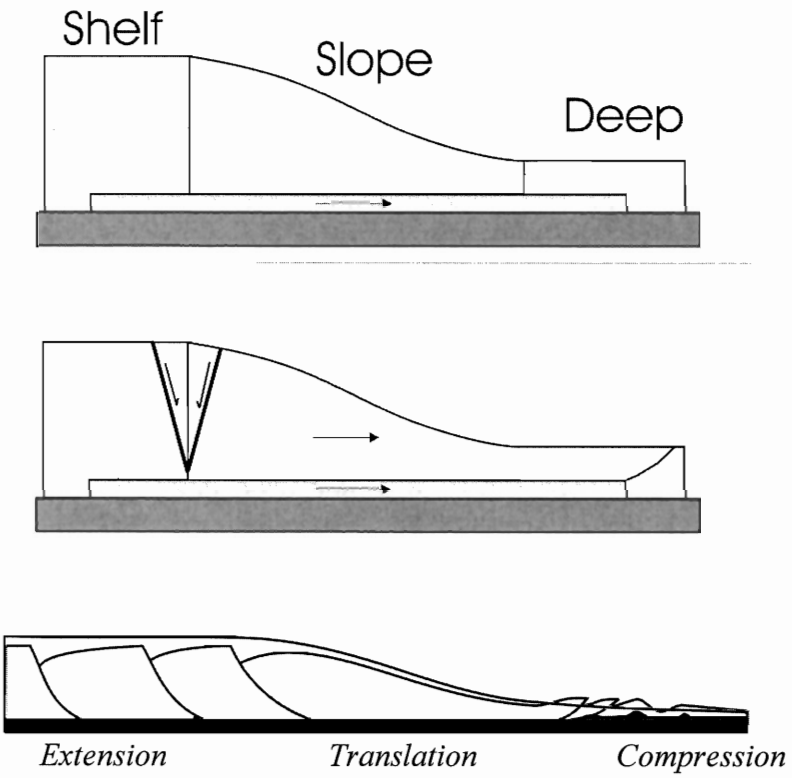

Figure 1.5: Initiation of deformation of overburden at the shelf-slope break. As silicone flows to the deep, extensional features develop in the shelf while compressional features in the deep. The slope section glides as a relatively undeformed internally unit (After Gemmer, 2004, bottom image by C. Krezsek).

Three kinematic domains develop at the initiation of deformation and are observed throughout the model's evolution of all models: extension, translation, and compression. Thus, extensional features such as grabens are observed in the shelf region while compressional features such as folds and thrusts are located in the deep basin region. The slope region is in the translational domain, and experiences some extensional features and large portions of it move basinward as relatively undeformed rafts. The silicone can rise in areas of weakness where the overburden is thinned (e.g., where grabens exist), creating reactive diapirs.

1.5 Tectonic Features associated with Salt Dynamic Processes

The terminology associated with salt tectonics is extensive and used in different contexts with various meanings. For this reason, the salt structures and their associated sedimentary features discussed in this thesis will be identified and explained here with definitions used in this thesis. Examples are given from cross-sections sections of the experiments, which are discussed in chapters two and three. All sections of the models can be seen in Appendix I.

The natural example which the physical models are made to represent is the named here the prototype. Overburden refers to the overlying sediments in the prototype, and sand in the models. Weak substratum refers to the underlying salt in the prototype and silicone in the models. Analogue materials used are discussed in chapter two of this thesis.

Deformation is diffuse in the first stage, which then focuses and evolves into narrow, elongate grabens. Brittle deformation is an instantaneous process, and its style depends on the strength of the overburden. Gravitational instability created by differential loading triggers a thinning of the overburden, accommodated by extensional structures such as grabens. These down-thrown blocks are bound by conjugate normal faults and relatively undeformed uplifted blocks, named horsts (Fig. 1.6).

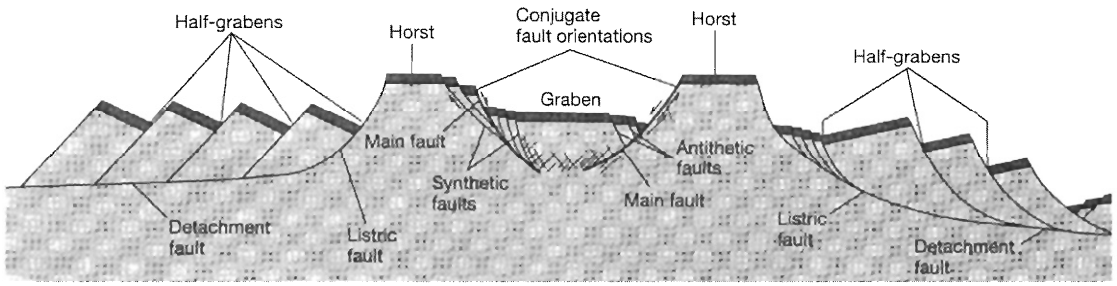

Figure 1.6: Systems of faults associated with grabens (Twiss & Moores, 1992)

Half grabens are bound by normal faults on only one side. The faults are typically listric (i.e. concave upwards) which straighten out and become parallel to a ductile detachment surface. Formation of grabens causes a thinning in the overburden, which in turn causes the rising of the underlying salt. Grabens in the model cross sections represent the early stage of deformation in response to extensional strain (Fig. 1.7). The graben will evolve depending on sedimentation rates (or lack of sedimentation).

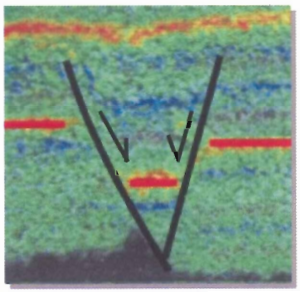

Figure 1.7: Graben in a cross section from experiment 3-7. Black lines are faults, and red are horizon markers. Black area at base is a small reactive diapir.

In thin-skinned gravity-driven systems, deformation of brittle overburden underlain by a ductile layer (e.g. salt) is characterized by growth or listric fault systems (e.g. Burrolet, 1975; Bally et al., 1981; Roberts & Yielding, 1994). Pre-faulting and syn-faulting sediments in the hanging wall are stratabound against the footwall by a listric fault. Thickening of syn-kinematic strata towards the listric fault indicates fault movement (Bally et al., 1981). If the hanging wall strata along the listric fault is displaced rollover anticlines are formed (e.g. Gibbs, 1984). Salt or welds are at the base of rollovers. Hanging wall strain in a rollover anticline is accommodated by a complex array of planar and listric normal faults developed around its crest (Gibbs, 1984; Mc Clay & Ellis, 1987). The ages of fault activity in these systems generally decreases towards the

boarder listric fault, but their timing overlaps considerably (Mc Clay, 1990; Mc Clay & Ellis, 1987; Mauduit & Brun, 1998; Imber et al., 2003).

There are two types of listric faults in growth fault systems, defined by their dip relative to the orientation of hanging wall displacement (e.g. Mauduit & Brun, 1998). The slope orientation of gravity displacement fields due to gravity spreading are referred to as basinward dipping growth fault (BGF) (or downslope) systems or landward dipping growth fault (LGF) (or upslope) systems.

Basinward dipping growth faults require movement of all hanging wall strata along the entire fault length during displacement. The hanging wall block must move at a higher velocity than its footwall for a BGF to occur, requiring efficient gliding of the hanging wall block on the detachment surface. Landward dipping growth faults dip in the opposite direction of the gravitational spreading (Fig. 1.8). Conflicting shear senses constrains displacement on these faults. LGFs occur only if the footwall block moves faster than the hanging wall (e.g. Mauduit & Brun, 1998). Thus, landward dipping growth faults indicate inefficient gliding of the hanging wall block. In LGF systems the hanging wall strata, which dips at steep angles at the flattened part of the listric fault, glides very slowly downslope or does not move at all. The displacement rates are several orders of magnitude lower in these regions than near the footwall of an LGF. BGFs represent an earlier stage of deformation than LGFs. Figure 1.8 shows how starting from a graben a structure develops into a BGF, and later LGF. Whether or not BGFs and LGFs are seen in a model, and the timing at which these faults occur, depends on the sedimentation rates, as discussed in Chapter 3.

← *Shelf* *Deep Basin* →

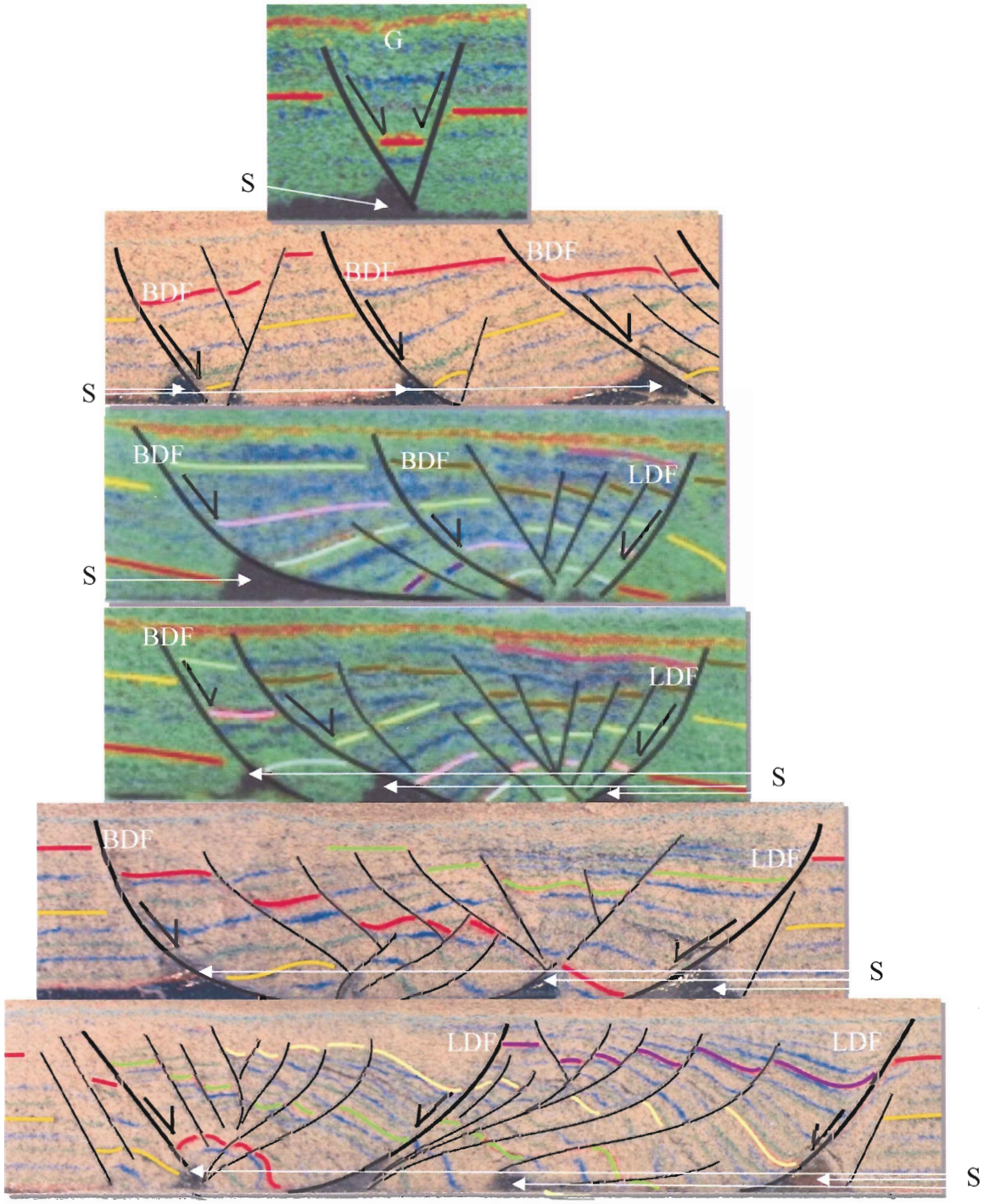

Figure 1.8: Structural evolution from graben (G) (top) to basinward dipping listric faults (BDF) (2nd and 3rd image) to landward dipping faults (LDF) (last three images, right sides). Salt rollers (S) are observed.

From experiments 3-7 and 4-3.

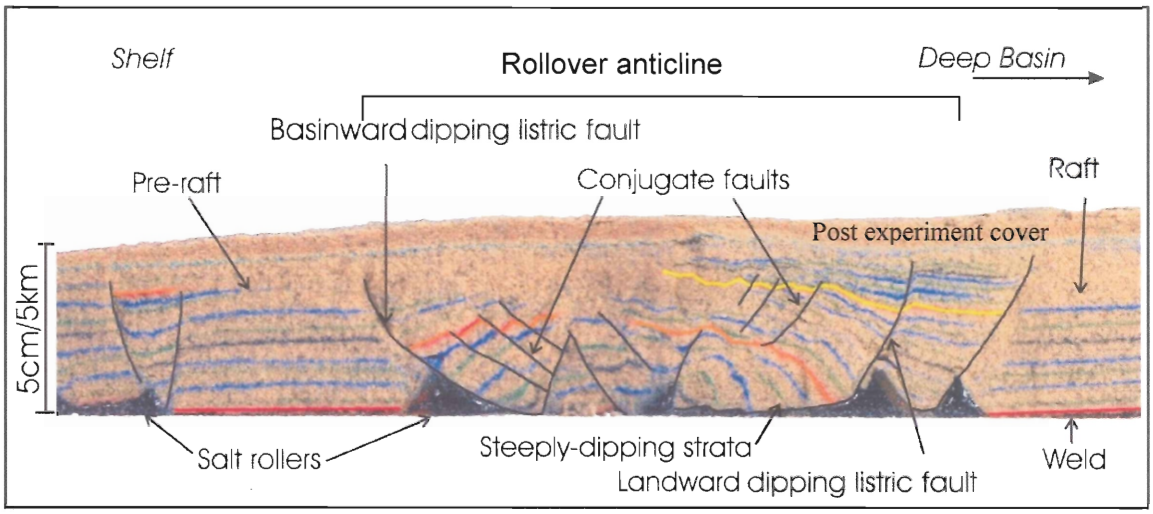

Figure 1.9: Part of a 2-D section from experiment 4-2 showing landward and basinward dipping listric faults.

Rafts are fault bounded blocks of relatively undeformed sedimentary sequences, typically representing former footwall blocks, which are no longer in contact with their original hanging wall blocks due to very high extension. Figure 1-9 has labelled sequences which appear to be rafts except that they are still in contact with the sedimentary sequences it began to separate from as pre-rafts. Because rafts move without internal deformation of the sequences, the paleoslope can be preserved. Often, rollover structures are bound by rafts which are welded at their base. Turtle structures are the result of salt withdrawal. Flanks of salt which uphold sedimentary sequences are later squeezed out, causing the sides of the sequence to subside and bend, leaving a turtle-shell shape in the sedimentary record.

Silicone structures are an important component of the experiments. Most salt structures can be further described beyond just 'diapirs', and are named based on their relative sizes and shapes (Fig. 1.10).

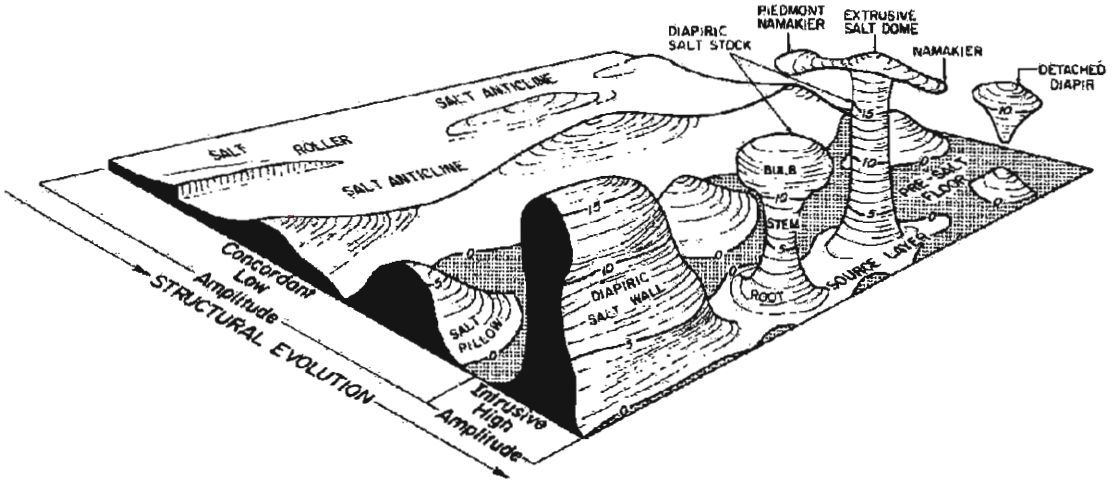

Figure 1.10: Salt structures (Twiss & Moores, 1992)

The most common salt structures described in this thesis are triangular shaped silicone rollers (Fig. 1.11). Theses are asymmetric, low-amplitude structures with two flanks, one of which is more gently dipping than the other (Bally et al., 1981).

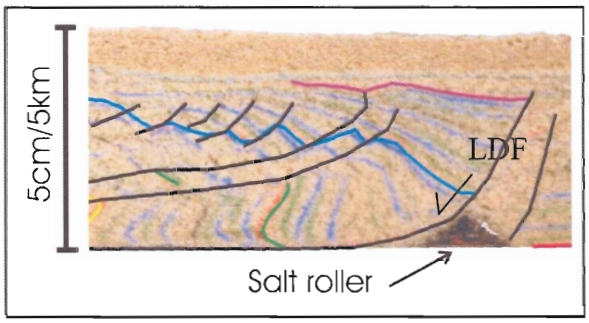

Figure 1.11: Silicone roller (the dark triangle) at the base of a landward dipping listric fault (LDF) in a cross-section section from experiment 4-2. Black lines are listric normal faults, dipping towards the shelf.

Some of the experiments have allochthonous silicone beyond the compressional-extensional domains previously discussed. These allochthonous areas were observed in only the experiments with tilted bases, but they would have occurred in all models if given enough time. That is, experiments 3-4, 3-5, & 3-7 were stopped before

they developed the allochthonous salt tongues. The tongues create a salt-tongue canopy, which could be observed from the surface of the experiment (Fig. 1.12).

Figure 1.12: Frontal salt tongue canopy, as seen from the surface of the model, near the end of the experiment, from experiment 4-2.

These experiments also had squeezed diapirs (Fig. 1.13), which occur when a previously extensional diapir becomes re-activated by later compression, causing the material to be squeezed upwards.

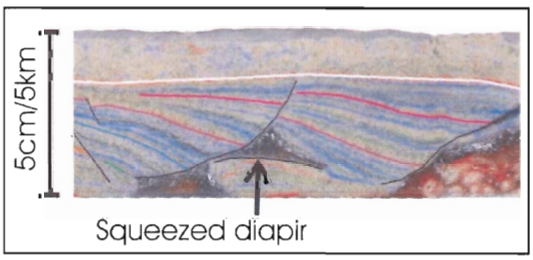

Figure 1.13: Squeezed diapir in a 2-D section from experiment 4-3

These faults in the sediments and salt structures are used to interpret the structural and kinematic evolution, as discussed in chapter three.

CHAPTER TWO: ANALOGUE MODELS AND TECHNIQUES

2.1 Analogue Modelling

Geological processes and the evolution of geological structures can be explored with analogue experiments by using model materials that simulate the deformation behaviour of natural rocks. With proper scaling of the model properties and material parameters, experimental results can be quantitatively compared to natural processes. As well as being a useful visualization for how structures evolve and interact on a geological time scale, properly scaled physical models are used to study controlling factors, processes, and feedback mechanisms in a constrained system. The use of analogue models for geological problem solving is extensive. It has proven to be a very useful tool for studies on all scales of geological processes and structures, from lithospheric scale processes to micro-scale crystal development (e.g. McClay, 1990, Koyi, 1997). Compressional, extensional, and associated deformation has been explored in detail with great success, and salt related experiments are no exception, as discussed in Section 2.3.

2.2 Historical Development

The first publication of analogue models was in 1815 by Sir James Hall (Hall, 1815), who used layers of tablecloths to model folding of layered sedimentary rock. Fractures, folds, and thrusts were explored as analogue modelling continued to develop through the nineteenth century (Favre, 1878; Daubre, 1879; Schardt, 1884; Cadell, 1887; Willis, 1893). A milestone in analogue modelling development was the formulation of scaling theory by M. King Hubbert in 1937. Hubbert outlined how models and prototypes can be systematically related using scaling factors. He recognized that scaling factors

allow for the already qualitatively useful models to be compared in a quantitative manner to the natural prototypes.

Analogue modelling continued to evolve over the twentieth century, as did the geological understanding of Earth. Models explored virtually all geological problems from grain to lithospheric scale. Gravity potential is the primary force driving plate tectonics, and so it is the primary force scaled in physical experiments. Centrifuges have been used to scale the field of gravity, in which materials with high cohesion can be used. Stronger materials allow for more time to set up models because they will not deform until put under the centrifugal forces. The size of models is limited when using centrifuges and the experimental set-up can be quite costly. Thus, experiments conducted under normal gravity are more cost efficient and less limited in the geometry of the models. By selecting materials with significantly lower strength, density, and viscosity (all lower than materials used in centrifuge models), the driving forces in normal gravity models can be scaled, as discussed in section 2.3. All of the models in this thesis are conducted under normal gravity.

Thanks to technological developments and material research (e.g. Lohrmann et al., 2003), analogue models continue to advance in their ability to yield quantitative information about geological processes. Recent advances include thermomechanical modelling (e.g. Cobbold & Jackson, 1992, & Wosnitza et al., 2001), 3D laser scanning (Grujic et al., 2002), computer tomography (Richard et al., 1989, Schreurs et al., 2002), pore pressure simulation (Nieuwland et al., 2000), and 2D/3D optical strain monitoring with particle imaging velocimetry (PIV) (Adam et al, 2005).

2.3 Overview of Salt Related Analogue Experiments

Salt tectonics has been studied in both compressional and extensional models, with a variety of materials under centrifugal and normal gravity. Complex geological processes in a basin system are non-linear, making them difficult to analyze from limited geological and geophysical data. Analogue modelling of salt related basin systems in ductile-brittle experiments can explore the complex interplay of processes. Hydrocarbon exploration focuses on structures in the brittle sedimentary rocks which overlay the salt sediments. Analogue modelling approaches have been proven to be an efficient tool to investigate brittle (sediments) and ductile (salt) deformation systems. Salt tectonic processes have been studied using analogue models and high resolution 3D monitoring and various boundary conditions, resulting in an improved understanding of salt-controlled basin formation on passive margins (e.g. Jackson & Vendeville, 1992; Vendeville et. al., 1994). These studies have significantly improved the understanding of extensional salt tectonics, such as graben formation, rollover anticlines, turtle strucutures, and block tilting (e.g. Mauduit & Brun, 1998; Vendeville & Jackson, 1992b). Only a few studies look at the development of syn-sedimentary structures in a passive margin sedimentary wedge from the extension domain in the shelf to the compressional domain in the deep basin (e.g. Fort, 2004; Vendeville, 2005). Numerical 2D modelling of margin-scale salt tectonic processes have proven to be insightful in the deformation mechanics of sedimentary wedges on passive margins due to gravity sliding and the effects of loading, isostasy and pore pressure (e.g Gemmer et. al., 2004).

2.4 Properties of Materials Used

In recent years, significant progress has been made in model material characterization and understanding control parameters of model deformation (e.g. Schellart, 2002; Lohrmann et al., 2003). Monitoring and measuring technology has become more sophisticated, and materials can be precisely measured and monitored (Koyi, 1997). Because both natural and analogue material properties are better understood, more appropriate materials are being used in analogue models. To model salt system dynamics two-layer experiments have been developed where a viscous material base is overlain by a brittle layer which is governed by frictional –plastic material behaviour.

It is assumed that evaporites behave as a perfect Newtonian viscous fluid (Byerlee, 1978). Newtonian fluids have a linear relation between stress and strain rate (Fig. 2.3). Finding an appropriate analogue material for salt is difficult because viscosity of salt 10^{17} to 10^{18} Pa · s (Römer& Neugebauer, 1991). The most common materials used to simulate salt in analogue models are silicone putties and rubbers, with various viscosities.

The silicone putties generally have higher densities than rubbers, and are commonly used to model lower crust deformation. The silicone rubber used in this thesis is a silicone elastomer, polymithylsiloxane (PDMS) by Waker, commercial name: El Polymer NAUS. PDMS is a visco-elastic fluid, with a mainly linear stress / strain rate relationship. At room temperature, the effective viscosity is 5×10^4 Pa and a density of 0.99 g/cm^3. PDMS has been used in other analogue modelling laboratories (e.g. Vendeville & Jackson, 1992 a & b)

Brittle rock, such as sandstone, deforms according to its shear strength, and the coefficients of internal friction and cohesion (Koyi, 1997). Sediments and sedimentary rocks generally show non-linear stress strain behaviour, with strain hardening and softening (e.g. Lohrmann et al., 2003). Although oversimplified, brittle rocks can be described with a Mohr-Coulomb criterion of failure (Byerlee, 1978). Mohr-Coulomb materials act elastically before failure, frictional-plastically after failure peak (fracture), and stabilize at the formation of a fault. These materials are contolled by the amount of pressure exerted by loading. Coulomb fracture criterion is defined by,

$$|\sigma_{cs}| = c + (\tan \Phi)\, \sigma_n \qquad (2.1)$$

where, σ_{cs} = critical shear stress, c = intercept, (tan Φ) = slope of the line, and σ_n = normal stress (Twiss & Moores, 1992).

Dry, granular materials are commonly used in analogue experiments under normal gravity to simulate brittle rock behaviour, because these materials show similar non-linear stress-strain behaviour. The experiments in this thesis use fluvial silica sand from Shaw Resources, Nova Scotia, Canada. The grains sizes are symmetrically distributed, (Fig. 2.1). Individual grains are rounded to subangular grain shapes, which allows for realistic shear zone formation.

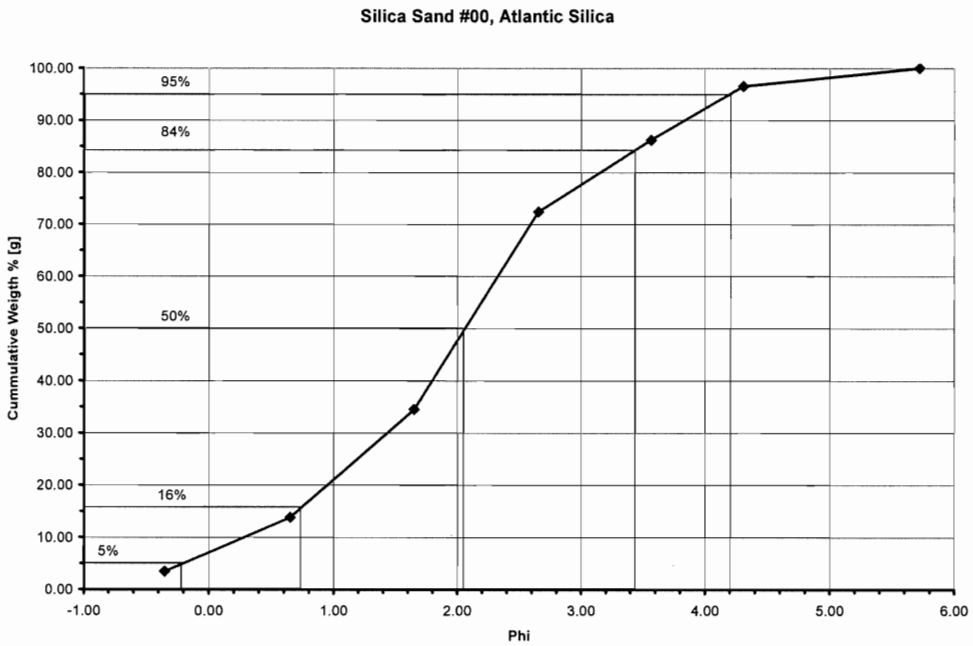

Figure 2.1: Typical grain size distribution of the fluvial sand used
(Graph by Gesine Adam & Sheila Ballantyne)

The grain size is measured in phi (ϕ), which is defined as:

$$\phi = [-\log_{10}(d / d_o)] / [\log_{10}(2)] \quad (2.2)$$

where d=diameter of the sand grain in millimetres. The grain size is determined by completing a series of sieving tests, in which the grains are sorted by size and then weighed.

Mechanical properties of sand in analogue experiments are strongly controlled by their mode of deposition (Lohrmann et al., 2003). To provide uniform mechanical properties in the models, specifically compaction, all of the sand material is sieved on to the experiments. The sieving procedure is described in Section 2.6.

In some experiments, finer sand and glass beads are used to model different natural materials, such as relatively weaker layers. The experiments for this thesis use only the silicone rubber, silica sand, and coloured silica sand (Fig. 2.2). The coloured

sand is used to create marker horizons for the each of the sieving / sedimentation intervals events (discussed in Section 2.6).

Figure 2.2: Materials used in analogue models at Dalhousie University. This thesis uses only the silicone rubber, fluvial silica sand, and coloured fluvial silica sand.

2.5 Scaling of Analogue Models

Scaling is crucial in making an analogue model quantitatively comparable to natural prototypes. The model is scaled such that the forces, time and geometric elements are proportionate to those in the prototype by a defined scaling factor. Scaling makes quantitative comparisons between the model and prototype possible.

Scaling theory was first established by M.K. Hubbert in 1937. He showed that there are three levels of similarity between the model and prototype: geometrical, kinematic, and dynamic.

Geometrical Similarity: If all corresponding lengths are proportional and corresponding angles are equal, the model and prototype is geometrically similar

(Hubbert, 1937). The ratio between lengths of the model and prototype must be constant and applied to all the length units in the model (Koyi, 1997).

Kinematic Similarity: If deformation and structural evolution in the model and prototype are geometrically similar and undergo proportionally equal changes in shape and position, they are kinematically similar. Temporal evolution in the model is proportional to that observed in the prototype.

Dynamic Similarity: When the model and prototype are both geometrically and kinematically similar they are also dynamically similar if the ratio between the acting forces on corresponding particles on each body is constant (Koyi, 1997). All of the models completed at the Dalhousie Salt Tectonics Laboratory are dynamically scaled.

In the models completed for this thesis, the following scale factors were determined. Each scale factor is the ratio between the value in the model and the corresponding value in the prototype or natural example. The asterisk indicates the value of a scale factor. Subscripts m is for model and p for prototype.

The first factor is length (L*), is a geometric scale factor derived from the physical parameters of sand and sedimentary rocks (i.e. density and cohesion) and gravity. In our models, 1 cm represents 1 km in nature, thus

$$L^* = (l_m/l_p) = (1 \text{ cm} / 1 \text{ km}) = 1 \times 10^{-5} \quad (2.3)$$

where l is length.

For the stress scale factor (σ^*), three components are considered: gravity (g^*), density (ρ^*) and length (L^*). Our models were completed under normal gravity, as in nature. Thus, the scale factor for gravity is one.

$$g^* = (g_m/g_p) = (9.8 \text{ m s}^{-1} / 9.8 \text{ m s}^{-1}) = 1 \quad (2.4)$$

For these models a density for sedimentary rocks of 2300 kg m^{-3} is assumed. The density of the sand used in the models is 1600 kg m^{-3}. The scale factor for density is therefore:

$$\rho^* = (\rho_m / \rho_p) = (1600 \text{ kg m}^{-3} / 2300 \text{ kg m}^{-3}) = 0.7 \quad (2.5)$$

Stresses experienced by the model are defined as:

$$\sigma = g \bullet \rho \bullet L \quad (2.6)$$

and thus, the scale factor for stress is:

$$\sigma^* = (g_m/g_m)\ (\rho_m/g_p)\ (L_m/L_p) = g^* \bullet \rho^* \bullet L^* = 1 \bullet 0.7 \bullet 1 \times 10^{-5} = 7 \times 10^{-6} \quad (2.7)$$

Now that stress is defined, the strain rate can be found. The brittle overburden (i.e. sand in the models) obeys the Mohr-Coulomb criterion of failure, and thus is not time dependent. For this reason, sand is not considered when determining the strain rate of the model. Salt sediments behave as a Newtonian fluid. The silicone used in the models is a viscous-elastic material (Weijermars, 1986). However, within the strain rates experienced in this study (typically about 10^{-5} s^{-1}), it can be assumed that the silicone behaves as a Newtonian fluid. For such materials, the strain rate depends on the applied stress and the viscosity of the material. As depicted in Figure 2.3, because silicone has lower viscosity than salt, less force is required for the same strain rate. This property allows analogue models to use less force and experience deformation in less time.

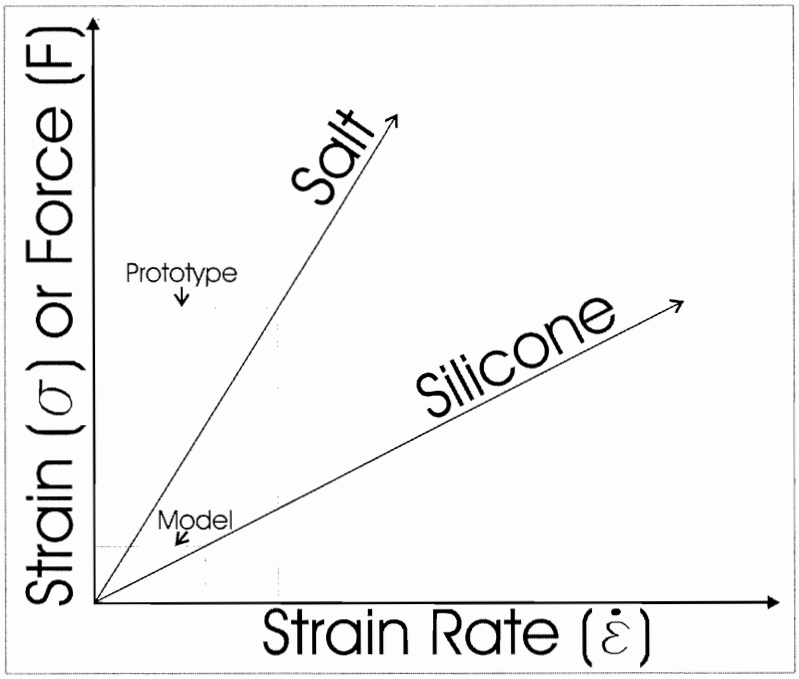

Figure 2.3: Strain vs. strain rate on for salt and silicone, based on viscosity (slope of the line) of the materials. (After Twiss & Moores, 1992)

The salt viscosity can vary by one to two orders of magnitude, depending on factors such as crystal shape, size, and fluid inclusions. For modelling salt related systems, salt viscosity is generally assumed to be between 1×10^{17} Pa s^{-1} and 1×10^{18} Pa s^{-1} (Costa & Vendeville, 2002). The large difference in values causes problems for scaling the models, particularly for time constraints. The rheological equation for dislocation/diffusion creep of salt needs to be improved before this issue will be resolved. If the higher value of 1×10^{18} Pa s^{-1} for salt viscosity is assumed, and the silicone used has a viscosity of 1×10^{4} Pa s^{-1}, the viscosity scale factor η^* is:

$$\eta^* = (\eta_m / \eta_p) = (1 \times 10^4 \text{ Pa s}^{-1} / 1 \times 10^{18} \text{ Pa s}^{-1}) = 1 \times 10^{-14} \quad (2.8)$$

The strain rate ($\dot{\varepsilon}$) is related by the stress and viscosity, such that,

$$\dot{\varepsilon} = (\sigma/\eta) \quad (2.9)$$

and the scale factor for strain rate is:

$$\dot{\varepsilon}^{*} = (\sigma_m / \sigma_p) / (\eta_m / \eta_p) = (\sigma^*/\eta^*) = (7 \times 10^{-6})/(1 \times 10^{-14}) = 7 \times 10^{8} \quad (2.10)$$

Thus, the model deforms 700 000 000 times faster than the prototype.

Time (t) is defined as the inverse of the strain rate factor:

$$t^* = (1/ \dot{\varepsilon}^{*}) = 1 / 7 \times 10^{8} = 1.4 \times 10^{-9} \quad (2.11)$$

Therefore:

1 hour in model = 1.4×10^{9} hours in prototype

(1.4×10^{9} hours = 159 817 years or ~ 160 000 years) (2.12)

If the lower value for salt viscosity is used, the models would indicate that the prototype develops one order of magnitude faster then the above answer (i.e. 16 000 years). This is an issue that still needs to be resolved. The larger value for viscosity is assumed for the models in this thesis.

In salt systems along passive continental margins another important parameter are sedimentation rates. On the Scotia Slope, the sedimentation rates on the Scotian Slope and similar systems are thought to be in approximately 1mm/year. Two of the models experienced high sedimentation rates of 0.5 cm / hour. This corresponds to 500 m of sediments over 160 000 years (i.e. sedimentation rate of ~ 3 mm/year). The other two sedimentation experiments experienced low rates of 0.25 cm / 2 hours, which corresponds to 250 m in 310 000 years in nature (or ~ 0.8 mm/year). The slope in experiments with high sedimentation rates progrades towards the deep basin 1cm/hour (1km/160 000 years in nature). In low sedimentation rate experiments, the slope progrades towards the deep basin 1cm/ 2 hours (1km/31 000 years in nature).Experiments are also conducted with no sedimentation and no prograding slope (i.e. stagnation). All of

the experiments have an initial period where the shelf is aggraded at the appropriate sedimentation rate. In stagnation models, a high rate is used. This is discussed thoroughly in the next section. These three sedimentation rates and patterns allow for the end members and one intermediate condition to be explored.

2.6 Experimental Set-up

All of the experiments for this thesis were conducted at Dalhousie University in the Analogue Model Deformation Laboratory with the help of the Salt Dynamics Group. The experiments were conducted on a table top, with guide rails along its length. Two charge-coupled device (CCD) digital cameras are mounted from the ceiling, giving a stereoscopic view. The cameras are connected to a dedicated computer monitor the experiments. Photographic lights are also hung from the ceiling (Fig. 2.4).

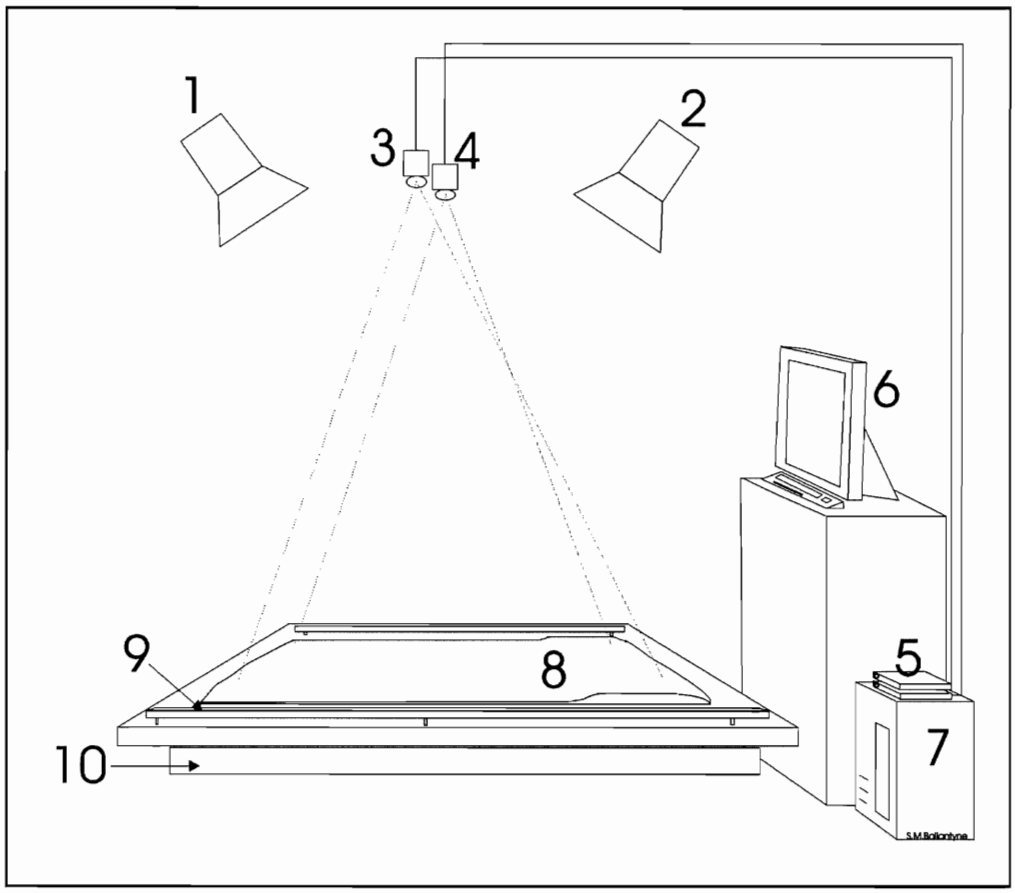

Figure 2.4: Diagram of the Dalhousie University Salt Lab.
1 & 2: Photo lights, 3 & 4: Cameras, 5: Controllers, 6: Monitor, 7: CPU, 8: Experiment, 9: Guide rail, 10: Experimental base. Length of experimental base is ~150cm.

In preparation, some of the sand is coloured with latex paint. All coloured sands are died, dried, and re-sieved to remove clumps. One part black-died sand is mixed with twenty parts plain sand to make the 'salt-and-pepper' pattern, crucial for the Particle Imaging Velocimetry (PIV) monitoring (see Section 2.6). Other sand colours, such as red, blue, and green, are made and used as marker horizons for successive sedimentation events. At the start of each sedimentation event, one of these colours is used, in a pre-determined order (e.g. green-blue-green-blue-red, repeat), and then covered by PIV sand to bring it up to a total of 0.5 cm for high sedimentation rate experiments, and 0.25 cm for low rate experiments. Because the coloured horizon markers are covered by PIV sand

at each sieving interval, the coloured sand is not interfering with the PIV monitoring software. The horizons are used when analyzing the post-experimentally cut 2-D sections. Sedimentation procedures and cutting of 2-D sections is described in the following paragraphs.

The set-up for each model starts with a 3cm wide border of uncoloured sand on the experiment table, which is later leveled to the same height as the silicone (1 cm) (Fig. 2.5). Within this boarder, the silicone is placed and allowed to spread over time under its own weight such that it becomes a 1cm thick sheet, typically 90cm x 60cm in area.

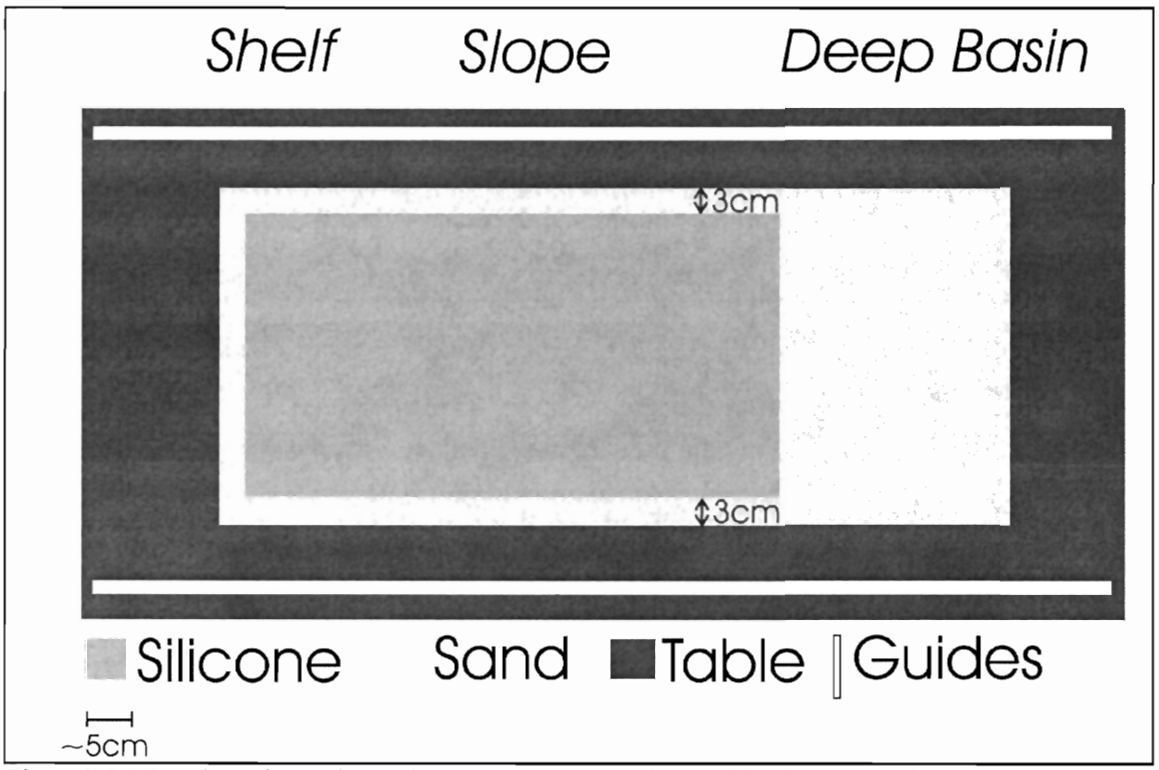

Figure 2.5: Map-view of experimental set-up, part 1: 3cm wide sand border surrounding 1cm thick silicone sheet, 90cm x 60 cm.

The amount of silicone required is determined by finding the volume created by the boarder (i.e. 90 cm x 60 cm x 1 cm = 5400cm^3) and multiplying it by the density of the silicone (0.99 g cm^{-3}). The amount needed in grams is then known. The appropriate

amount of material is then placed within the sand border in small pieces and left to fill the space as it flows under its own weight. It takes one to two days to allow the silicone to become a uniformly-thick sheet and allow trapped air to escape through rising bubbles. On one side of the experiment, where the deep basin will eventually exist, a 1cm thick layer of uncoloured, sieved sand is put down such that, typically 30cm long and the same width as the experiment (Fig. 2.5). This area of sand in front of the silicone sheet represents the sedimentary rocks of the deep basin at the seaward limit of the salt basin.

Once the silicone has spread out evenly, the entire experiment is covered lightly with PIV sand. All covering and sedimentation is done by sifting sand from a cup with drilled holes in the bottom and shaking it on to the experiment from a constant height and procedure to provide uniform mechanical conditions (i.e. compaction) of the sand. The first part of the shelf is then built up, by using the guide lines which run the length of the table (Fig. 2.6).

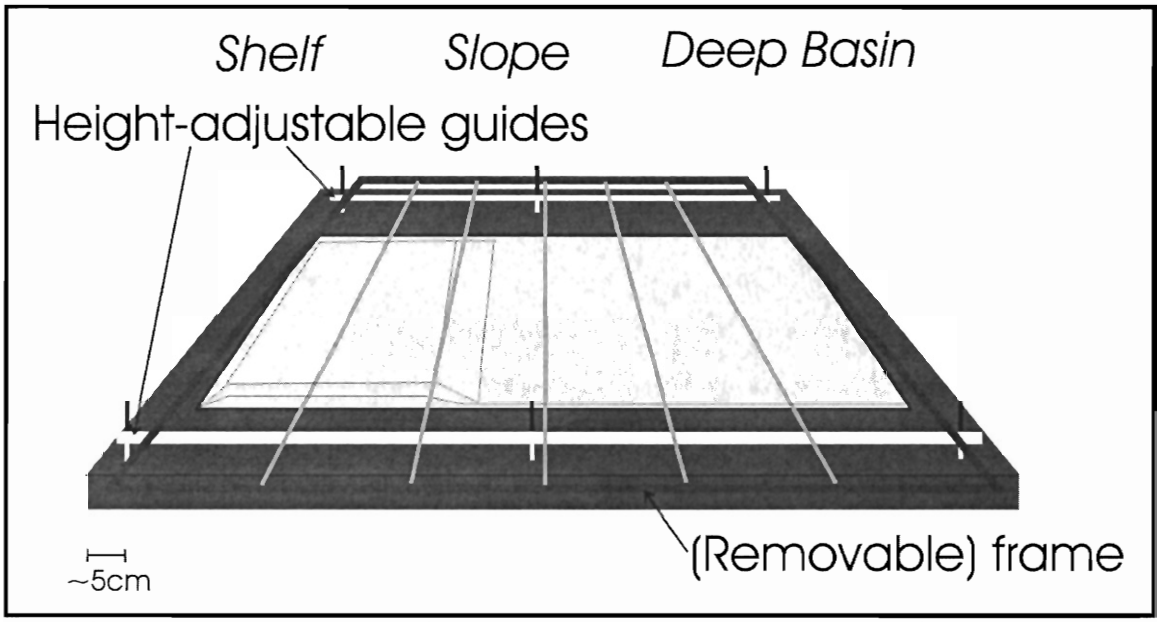

Figure 2.6: Side view diagram of guides and frame used to constrain amount of sedimentation.

The guides are adjustable in height. Tape measures run down the sides of the table to measure the length of the experiment and to define the location of the slope. A frame with ten level strings stretched across it, space 10cm apart, is placed on top of the guides above the experiment during the sedimentation procedures. The height of the shelf and slope location is constrained by adjusting the height of the guides and using the rulers and strings as a guide. After the first sieving event, monitoring of the experiment starts.

Each of the experiments in this thesis has a period of aggradation, in which the initial shelf geometry is built up to 4cm above the initial silicone layer. This gradual build-up is more realistic than starting with the shelf wedge on top of the sediments without previous deformation. The shelf is built up at 0.5 cm for high sedimentation and stagnation experiments, and 0.25 cm for low sedimentation rate experiments, per sieving event. During shelf build up procedures, as well as later sedimentation intervals, material is also added to the slope such that it advances basin-ward by 1 cm per sieving event (Fig. 2.7). Once the shelf has reached a thickness of 4 cm (equivalent to 4 km in nature) above the silicone, the guides are now no longer raised for sieving events, and only the shelf continues to grow as the slope migrates towards the deep basin (blue in Fig. 2.7). The stagnation models (experiments 3-5 and 4-1) do not experience sedimentation beyond the shelf and associated slope build up.

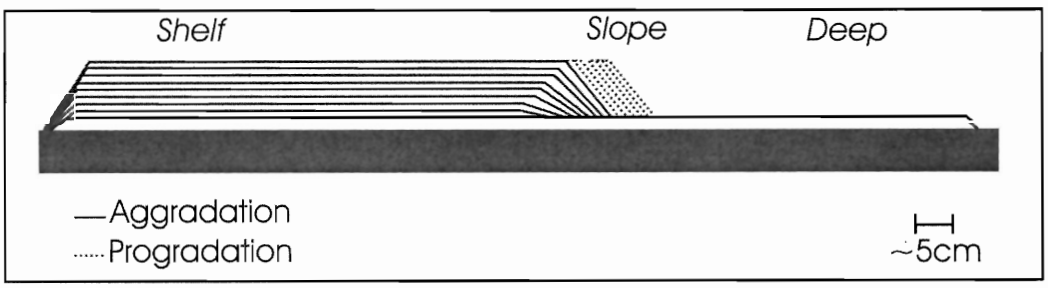

Figure 2.7: Diagram of initial aggradation of the shelf and following progradation of the slope. Silicone underlies the sedimentation within the black-outlined area at the base, from the shelf to the beginning of the deep.

As the slope moves towards the deep basin, grabens developing in the shelf area are filled with a thickness of sand depending on the sedimentation rate. If a graben is deeper than the rate for the experiment (i.e. 0.5 cm or .25 cm) it would require more than one sedimentation procedure to be filled. Grabens on or behind the slope experience sediment deposition, but the grabens basinward of the slope do not.

The two models which are developed without sedimentation (3-5 and 4-1) begin the same way with the build up of the shelf, but once it has reached a thickness of 4 cm, no further sedimentation is carried out.

Experiment	**3-5: Stagnation (flat base)**	**4-1: Stagnation on a 5°tilt**	**3-7: (Low) Progradation (flat base)**	**4-3: (Low) Progradation on a 2°tilt**	**3-4: (High) Progradation (flat base)**	**4-2: (High) Progradation on a 2° tilt**
Area of silicone	108x38 cm	90x60cm	100x60 cm	93x65 cm	100x66 cm	86x63 cm
Shelf build up	4.0 cm	4.0 cm	4.0 cm	4.0 cm	4.0 cm	4.0 cm
Slope progradation	none	none	1cm/2 hours	1cm/2 hours	1cm/hour	1cm/hour
Sedimentation rates	none	none	0.25cm/2 hours	0.25cm/2 hours	0.5cm/hour	0.5cm/hour
Duration of experiment	72 hours	63 hours	56 hours	148 hours	98 hours	71 hours

Table 2.1: Parameters of the three experiments conducted in this thesis (4-1, 4-2, & 4-3) and three previously completed experiments (3-4, 3-5, & 3-7).
Stagnation: shelf build-up only; Low: 0.25cm/2hours sedimentation rate;
High: 0.5cm/hour sedimentation rate.

Three experiments were conducted with the experimental base tilted at 5° (experiment 4-1) and 2° (experiment 4-2 & 4-3). This was achieved by placing wooden blocks under the shelf end of the experimental base so that the desired angle was achieved (Fig. 2.8).

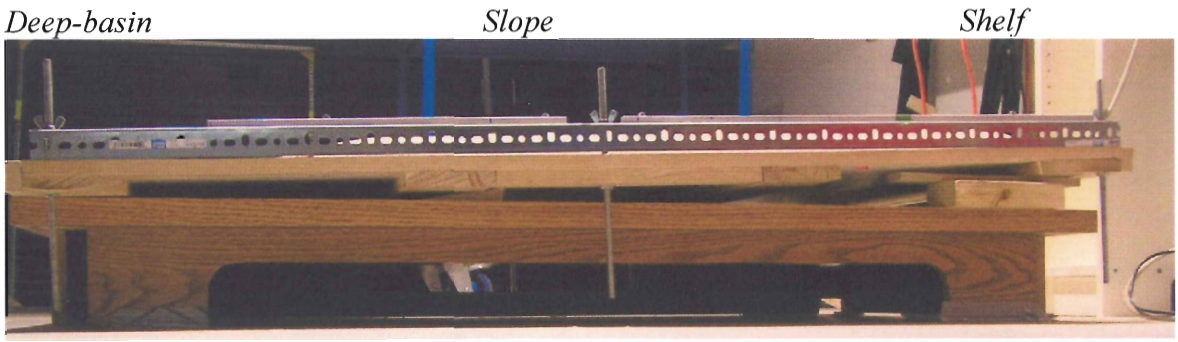

Figure 2.8: Experiment with highly sophisticated tilting of base. Length of experimental base is ~150cm.

The experiments are considered complete and monitoring is stopped when either the slope reaches the end of the experimental base, such as in experiments 4-1, 4-2 and 4-3, or when deformation is significantly slowing down due to complete feeding and sliding of silicone up to the basinward limit, such as in experiments 3-4, 3-5, and 3-7 (i.e. no more grabens or silicone diapirs develop). If left for more time (i.e. months) the silicone would be almost completely driven out of the system and of the initial basin area. The entire experiment is covered with a final colour marker horizon to leave a record of the experiment surface, and then is uniformly buried with a few centimetres of sand to stop any further movement of silicone. The sand is then wetted by spraying it with two to three litres of water. High cohesion of wet sand allows for sectioning, as discussed in the next section.

2.7 Particle Imaging Velocimetry (PIV) Monitoring

PIV is a non-intrusive optical monitoring technique in which the displacement and velocity of movement is accurately and instantaneously observed. The spatial resolution of PIV is determined by the camera resolution, field of view and correlation algorithms (Adam et al., 2005). The experiment is monitored with two digital cameras in stereo set-

up (Fig. 2.4). Calibration of the camera set-up before each experiment provides the mathematical mapping functions to calculate the 3D topography and 3D surface flow from the stereo images. This calibration is done with a calibration plate, which is a white board with a series of evenly spaced block dots on two different levels. The calibration board is placed on top of the initial experiment set-up, using the guide rails. A photo is taken by each camera. The experimenter then selects a reference dot on the computer screen in both images. The software then identifies all of the corresponding dots in each picture for the entire calibration plate, which takes up the entire field of view. The upper and lower level dots are calibrated in the same manner.

Once the first sieving procedure is complete, the monitoring begins. The digital cameras image the experiment with time-series photos, taken once per minute (the frame-rate) over the time of the entire experiment. Davis® Strain Master software detects and traces patterns on the surface of the experiment by the PIV sand. It determines the displacement of a given sub-sample by matching the best pattern made by the PIV sand from one photo to the next. If the program worked by tracing a single particle as it moved throughout a model's evolution, it would not be possible to add sediments during the experiment because the particle would be buried. By using best-matched patterns created by the salt-and pepper PIV sand, subsequent sequences of layers can be deposited (such as when sieving events occur) without disruption of monitoring. A displacement vector is determined for each sub-sample for the complete image by cross-correlation of the pattern in the sub-samples of successive images. The peak correlation is most likely the displacement vector of the sub-sample. In this way, the incremental and cumulative displacement field of the entire experiment is calculated. The data yield the finite and

incremental information for the vertical subsidence and uplift, horizontal displacement, velocity, shear strain, plain strain, and strain rate for the model. This digital information is directly comparable with results of numerical models.

2.8 Cross Sections

The final step of the experiment is to cut it lengthwise at 5 cm intervals (Fig. 2.9). The material in front of the cut is discarded and the exposed surface is cleaned using pressurized air and photographed.

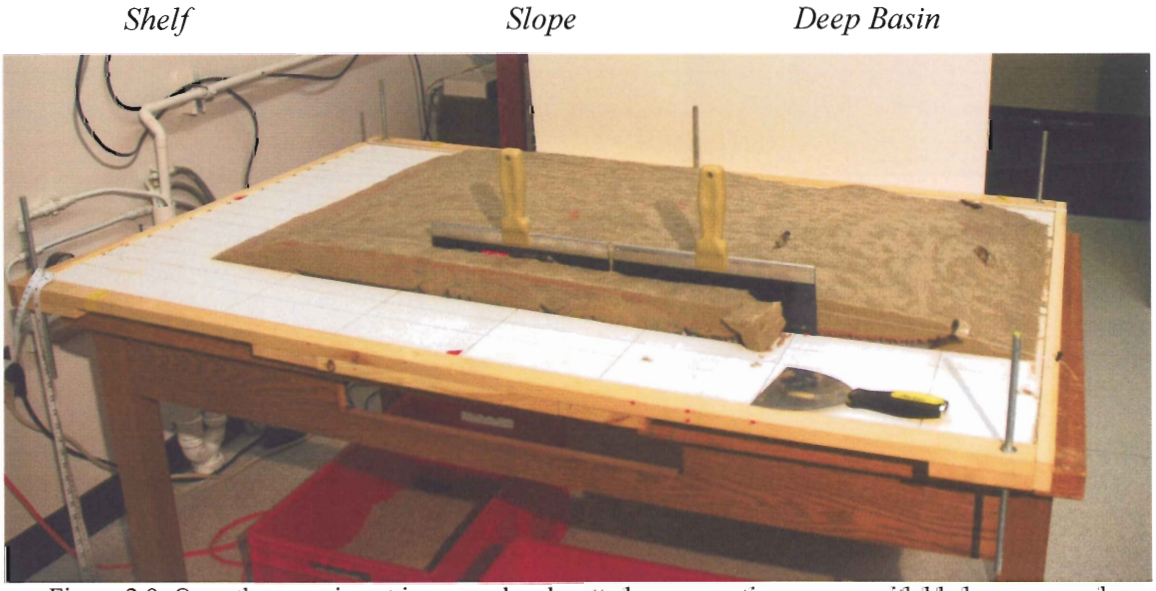

Figure 2.9: Once the experiment is covered and wetted, cross-sections are cu with blades, as seen above. The black lines on the base surface, running from shelf to deep basin, are spaced 5cm apart.

There is no detectable distortion caused by the cutting, however one must work quickly to prevent the silicone from flowing out of the model. Several photographs are taken of each section. These photos are digitally stitched together to generate the complete section. A stitched section can be interpreted in the same manner as a structural or seismic cross-section. All of the cross sections can be found in appendix I. The various coloured marker horizons used during each sieving event are marked and structural

features are identified. For clarity, the images of the sections are digitally enhanced in Photoshop®.

2.9 3-D Models

The stratigraphic horizons and structures can be extrapolated from one section to the next. Csaba Krézsek has completed and developed 3D models for the experiments using Petrel® software (Fig. 2.10). Because if the structural complexity and rapid change of strucutures along strike, the 3D model is constructed by using the interpreted cross sections as well as PIV deformation data, which gives information on the sequence of activity of individual faults. The work required to build one of these models is quite extensive, even with the aid of sophisticated software. Due to time constraints, 3-D models were completed for only one of the experiment in this thesis. These 3-D models are not included in this thesis. This remaining work is valuable, and will be completed in the future.

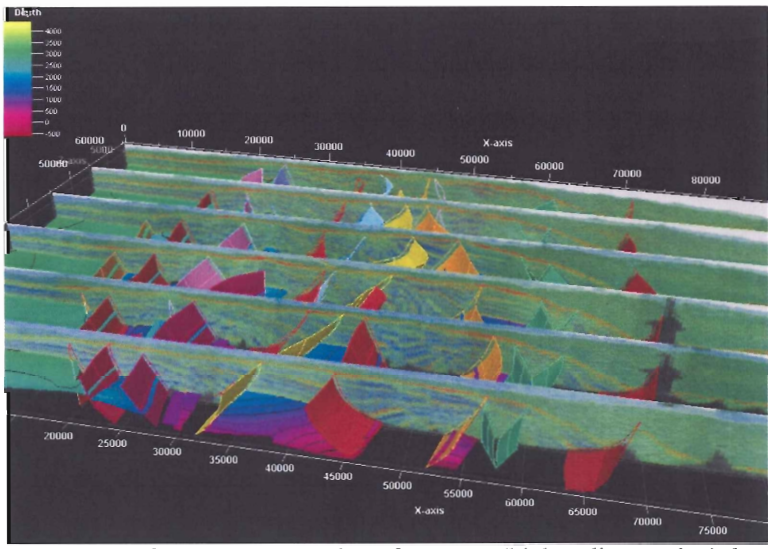

Figure 2.10: Part of a 3-D interpretation of exp. 3-4 (high sedimentation), based on the cross sections (green rectangles running ~ horizontal) and using PIV data. The coloured surfaces intersecting the cross-sections mark the surfaces of structural features, such as faults. (By Csaba Krezsek)

CHAPTER THREE: DESCRIPTION OF EXPERIMENTS

3.1 Description of Experiments in this Thesis

The complete series of cross sections and PIV data for the experiments is shown in appendixes I and II. By altering parameters such as sedimentation patterns and rates for individual experiments, as described in Table 2.1, different deformation styles occur. For each experiment, the key features observed are described here. Because the structural cross-sections are too large to be placed within the text with reasonable resolution, only characteristic portions are taken to highlight important structures. Similarly, only key images from the PIV strain data are shown in the text to explain the kinematic evolution of the experiments. By looking at appendixes I and II, the entire structural inventory and time-series data of the displacement data can be seen, which is extremely helpful in understanding the evolution of the experiments.

3.1.1 Stagnation on a Flat Base

Experiment 3-5 was conducted on a flat base. It experienced a shelf build-up phase such that the sediments are 4cm thick on top of the silicone layer. There was no further sedimentation after this stage simulating starved margin sedimentation after the initial shelf build-up stage. Aggradation followed by stagnation is dominated by the formation of structural and morphological grabens (Fig. 3.1). The grabens are cored by silicone, which start as reactive diapirs that can develop into passive diapirs if extension is high enough. Between the grabens are large horst blocks, many of which are welded at their bases in late stages. There is a complete lack of basinward dipping listric faults (BDFs) and landward dipping listric faults (LDFs) in this model.

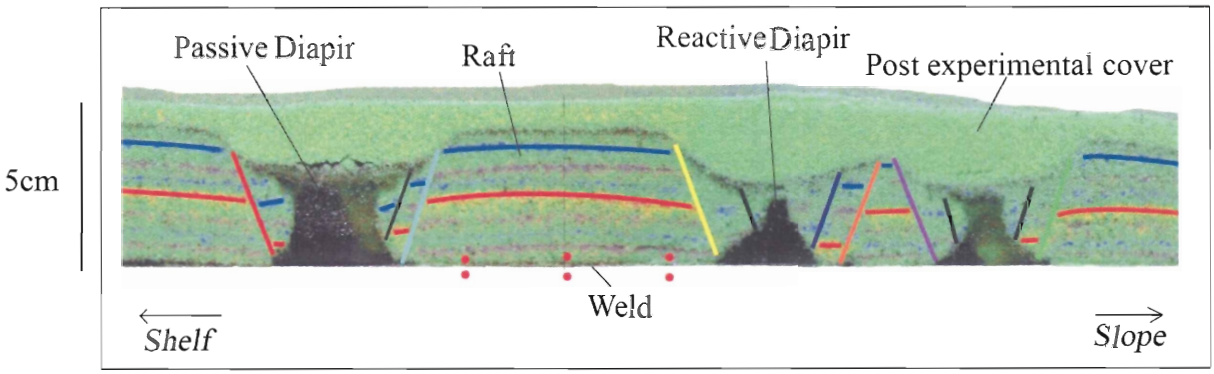

Figure 3.1: Part of a cross-section from experiment 3-5. Silicone diapirs (black areas) start as reactive diapirs (two features on the right side) and evolve to passive diapirs (silicone feature on left).

The PIV strain data for experiment 3-5 (Fig. 3.2 a-d) reveals that the deformation initiates at the shelf-slope break. Deformation begins as diffuse strain, which have the greatest strain and subsidence is at their cores. As extension continues, grabens develop, which also have strain and subsidence at their cores. Material is carried basinward in the form of hanging walls, foot walls, and rafts, causing the opening of features such as grabens. Silicone flows up where the overburden is sufficiently thinned, thus causing the greatest subsidence to move to the edges of the grabens. Because there is no prograding slope in the stagnation models, the shelf-slope break migrates back towards the shelf as material glides basinward. Thus graben initiation jumps back towards the shelf once the early grabens have reached the passive diapir stage (Fig. 3.2c&d).

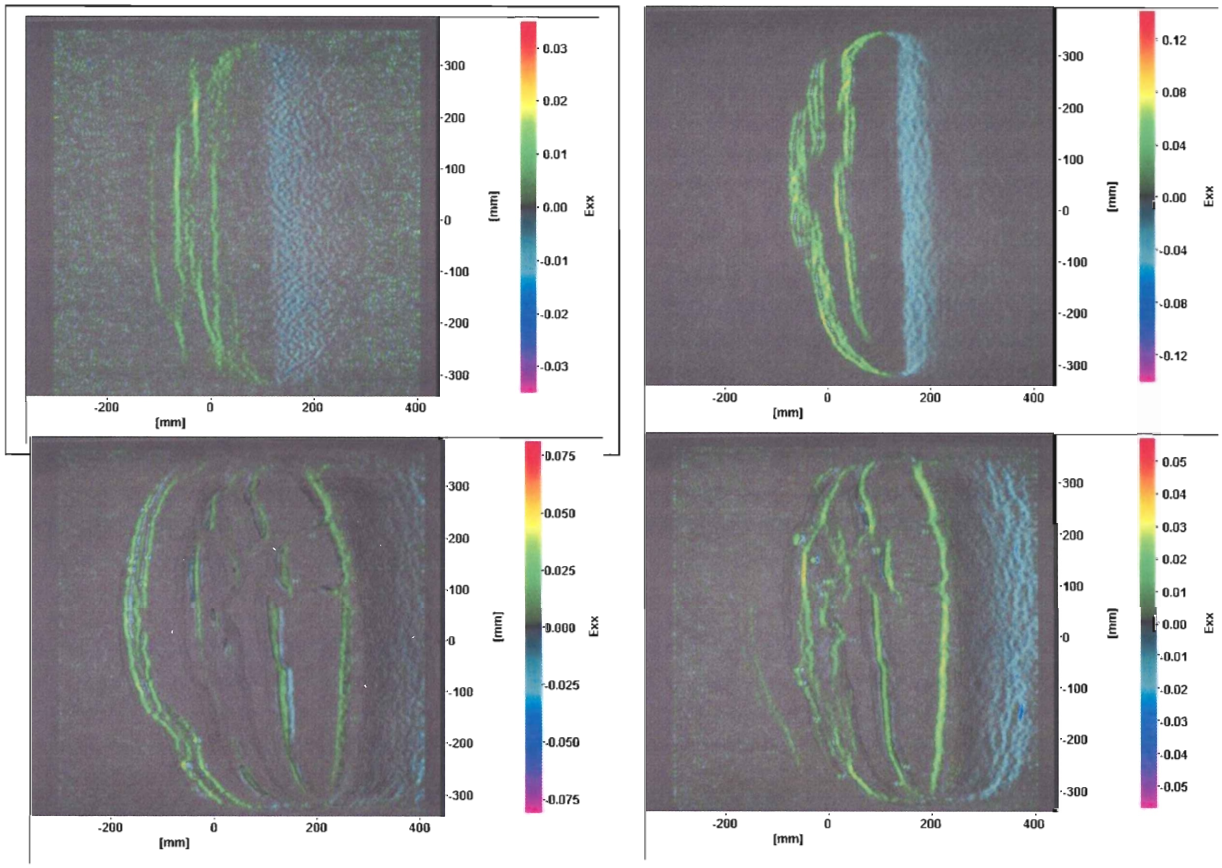

Figure 3.2: Incremental strain PIV data from experiment 3-5. a) Top left: early in development, showing diffuse deformation and graben formation. b) Top right: Grabens extend over time, and silicone rises. c) Bottom left: Once grabens have extended such that diapirs are passive, deformation migrates back into shelf area d) Bottom right: Grabens continue to extend, with the greatest strain along normal faults at their edges as silicone rises at their cores.
Please note colour scale bar is different for each image.

3.1.2 Stagnation on a Tilted Base

Experiment 4-1 was conducted with its base tilted 5°, which is 3° more than the other tilted-base experiments. This was created as an initial test to observe the evolution and limiting parameters when the model was tilted. A wedge was placed over the entire experiment, with a thickness of 4 cm at the shelf and tapering near the deep basin. No further sedimentation was done. Figure 3.3 shows a cross-section from experiment 4-1, which has similar features as those seen in experiment 3-5 (Fig. 3.1). Grabens, passive diapirs, and rafts are seen. The main difference between the flat base 3-5 model and tilted

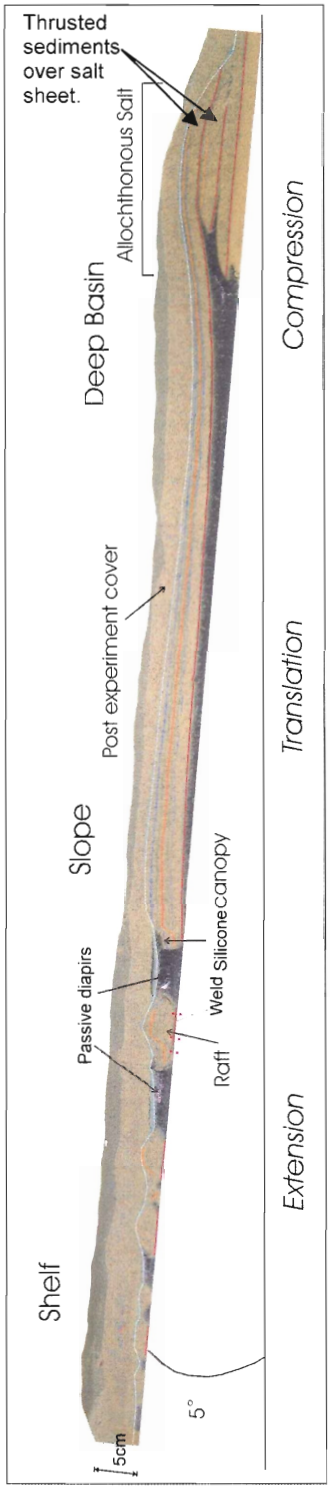

base 4-1 model is that in the frontal section of 4-1 a very large unfaulted sequence (i.e. a raft) of sand exists and is thrusted over the deep basin sediments by allochthonous salt sheets (Fig. 3.3).

Figure 3.3: Cross section from experiment 4-1. Symmetric grabens, passive diapirs, and allochthonous salt in the deep basin are characteristic of stagnation on tilted base models.

Although reactive diapirs are not preserved, it is assumed that the silicone would have been reactive before reaching the passive stage. All models would achieve allochthonous "salt" sheets if given enough time to deform.

Experiment 4-1 evolved in a similar manner as experiment 3-5 (aggradated shelf, stagnation), with diffuse strain followed by localized strain on fault structures until the silicone rises and strain continues to be localized as the major grabens form. Experiments 4-2 and 4-3, discussed later in this chapter, have allochthonous silicone features as well, and the PIV data for these two models is complete and described in Sections 3.1.4 and 3.1.6.

3.1.3 Progradation, and Low Sedimentation Rates on a Flat Base

In experiment 3-7, the same initial shelf build-up of 4cm as the other models was completed, with a prograding slope at 1cm/2 hours (1km/310 000 years in the prototype), and sedimentation rates of 0.25cm/2 hours (250m/310 000 years or ~0.8mm/year in the prototype).

The low sedimentation model on a flat base has passive diapirs (Fig. 3.4). As the slope progrades towards the deep basin, landward passive diapirs stop to grow and become sealed in the inner shelf area.

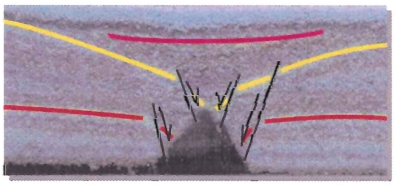

Figure 3.4: Part of cross section from experiment 3-7 showing passive diapir (black part) and graben (black fault lines). The tip of this diapir was at the surface of the experiment during main extension. (Model is 5cm thick)

Low sedimentation models also have late stage BDFs, which all have salt rollers at their bases and conjugate faults surrounding remnants from reactive diapir rise phase (Fig. 3.5a). Some LDFs are also observed, however they are less developed than the BDFs and occur in smaller quantities (Fig. 3.5b). These LDFs are formed through the expulsion of silicone.

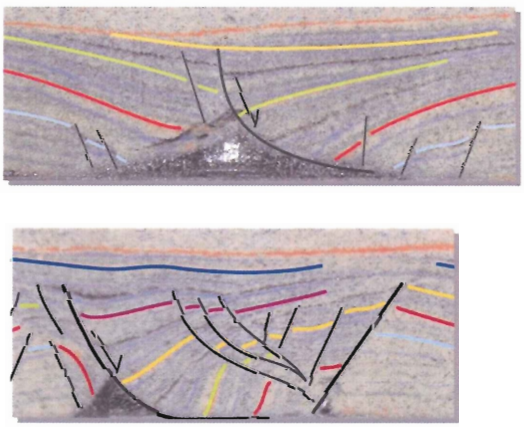

Figure 3.5: Parts of a cross section from experiment 4-3 (the same features are seen in experiment 3-7, but images for 4-3 is clearer). a) Top: Symmetric rollers on the flanks of a passive diapir b) Below: Early passive diapir developing a late basinward dipping listric growth fault rollover system with a keystone graben (Sediments are 5cm thick in images)

Deformation processes begin in the same manner as observed in experiment 3-5. The rise of diapirs is observed in 3-7. Deformation steps back (see bottom left image of figure 3.6) as the shelf slope break migrates towards the deep basin. Figure 3.6 shows a frame from the accumulated subsidence which follows a feature that evolves from a graben to a BDF.

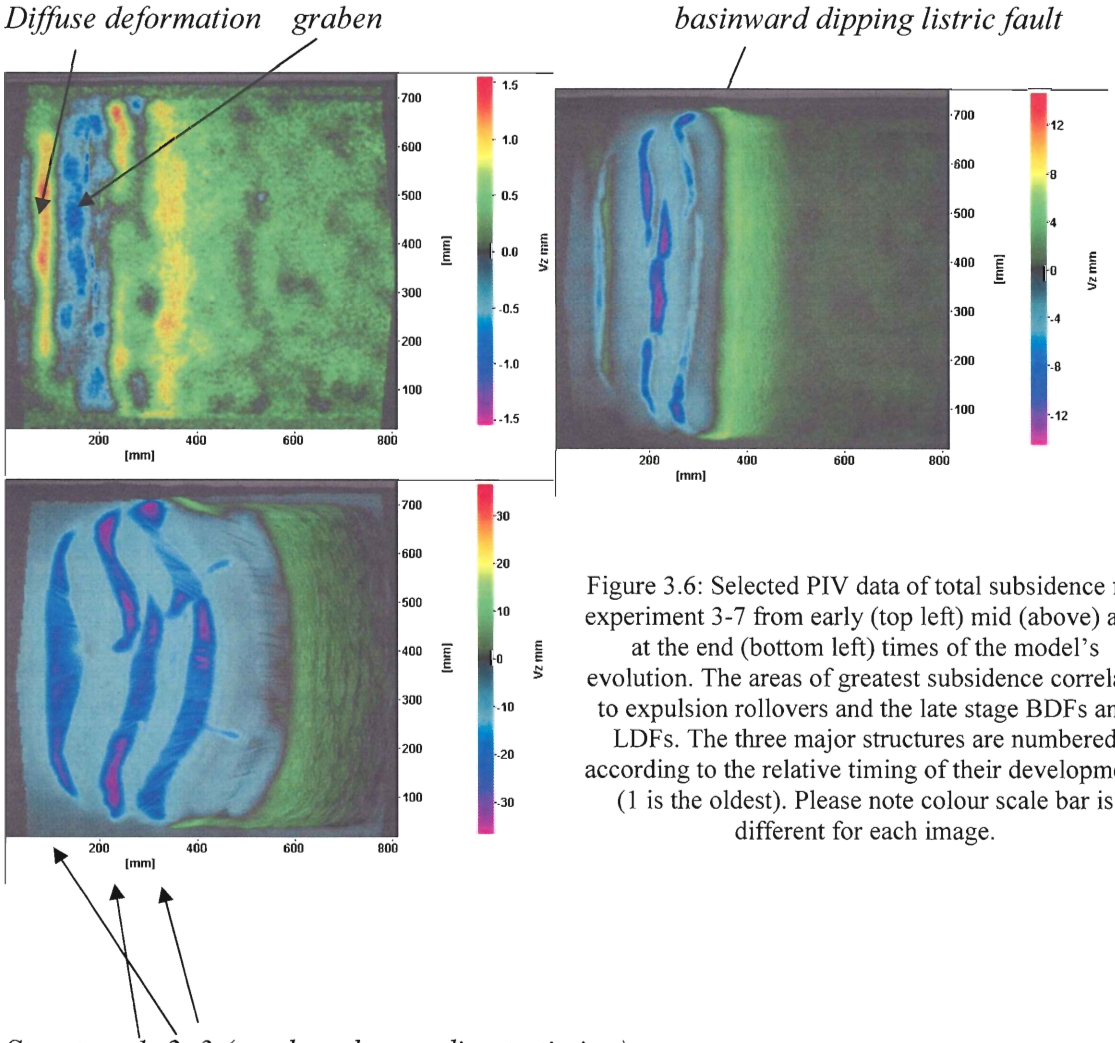

Figure 3.6: Selected PIV data of total subsidence for experiment 3-7 from early (top left) mid (above) and at the end (bottom left) times of the model's evolution. The areas of greatest subsidence correlate to expulsion rollovers and the late stage BDFs and LDFs. The three major structures are numbered according to the relative timing of their development (1 is the oldest). Please note colour scale bar is different for each image.

3.1.4 Progradation, and Low Sedimentation Rates on a Tilted Base

The final model completed for this thesis, experiment 4-3, experienced the same initial shelf build up, progradation, and sedimentation rates as experiment 3-7 (4cm slope, 1cm/2 hours prograding slope, 0.25/2 hours sedimentation). It only difference is that it

was conducted on a base tilted 2°. Structures in experiment 4-3 are very similar to those observed in 3-7. Figure 3.7 is a cross section from the middle of experiment 4-3. The structures in the appendix are clearer because the image is larger than the one shown here.

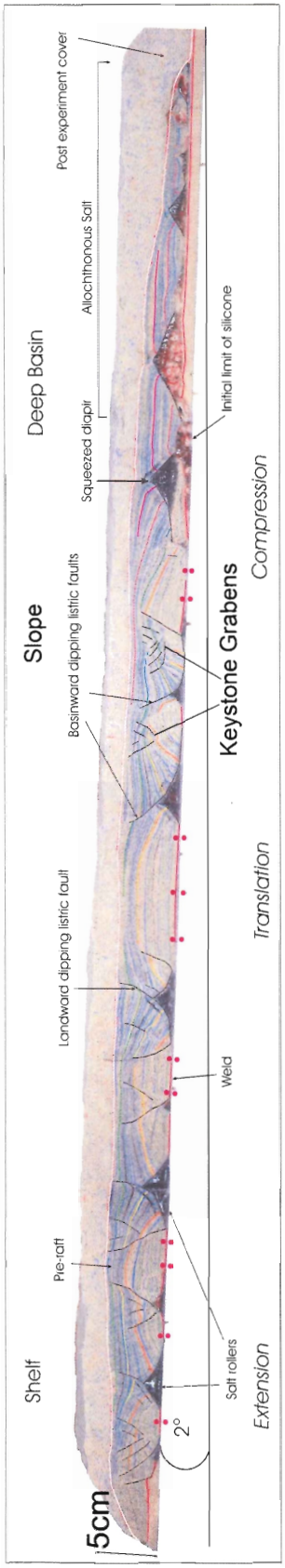

Figure 3.7: A cross section from the middle of experiment 4-3 showing rafts with welded bases, BDFs and LDFs, keystone grabens, allochthonous "salt" sheet, and reactive diapirs and a squeezed diapir.

This tilted base model with low sedimentation differs from its counterpart flat base model in that its late stage listric growth fault rollover systems are more developed, there is allochthonous silicone in the deep basin, expulsion rollovers and a squeezed diapir is present. Once again, it is assumed that the flat base model would show these features as well if sedimentation and progradation would continue to a similar stage. Thus, experiment 4-3 deformed much faster than experiment 3-7.

The PIV data for experiment 4-3 (Fig. 3.8) is similar to that of 3-7. It should be noted that although the colours in Figures 3.6 and 3.8 are the same, the scale is different (seen along the right sides of the images). Experiment 4-3 experienced more accumulated subsidence (shown as negative values

according to the scale bars). The positive values (shown in green) on the right side of the images in Figure 3.8 are the result of thickening due to shortening and the allochthonous silicone which was thrust up and over the frontal sediments. The same colouring is seen in Figure 3.6 for experiment 3-7, however, the scale is different once again. The positive relief in the front of experiment 3-7 is caused by the compressional features, such as small folds, in the deep basin area, and not by allochthonous silicone.

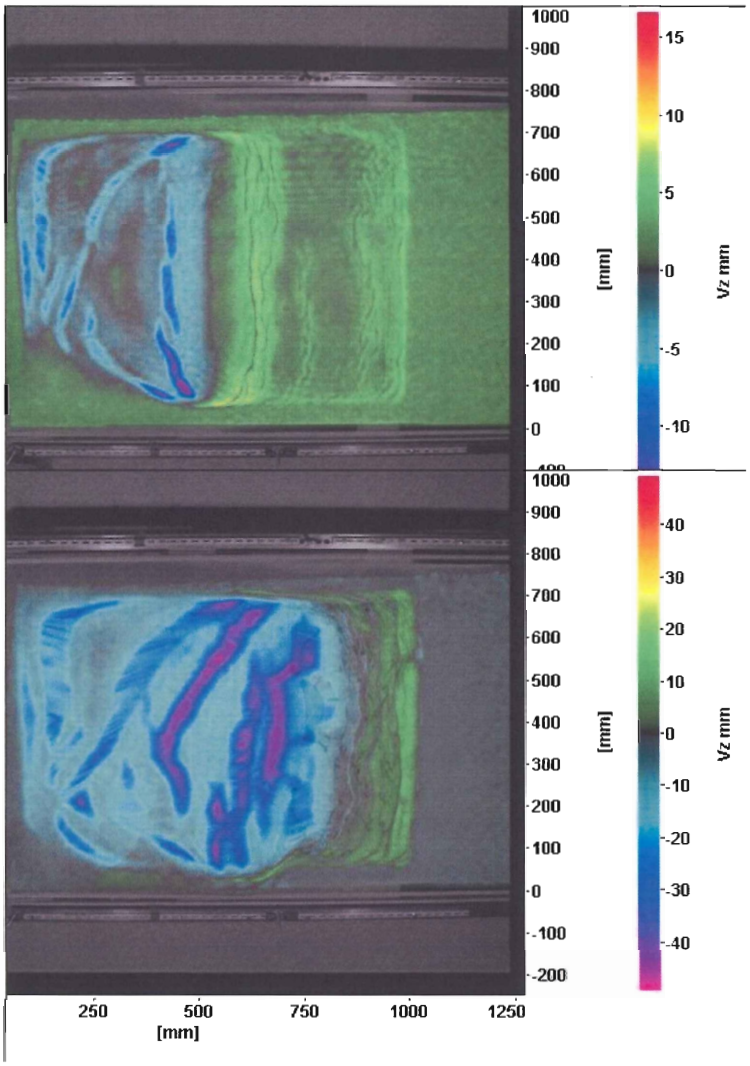

Figure 3.8: Selected PIV data of total subsidence for experiment 3-7 from early (top) and late (bottom) in the of the model's evolution. The areas of greatest subsidence correlate to locations of BDFs and LDFs. The frontal positive relief is due to the allochthonous silicone. Please note colour scale bar is different for each image.

3.1.5 Progradation, and High Sedimentation Rates on a Flat Base

Experiment 3-4, which was conducted on a flat base experienced the initial shelf build-up phase until the sediments were 4cm thick above the silicone layer. This experiment also experienced sedimentation at a rate of 0.5cm/hour (or 500m / 160 000 years or ~ 3mm/ year in the prototype) and a prograding slope at a rate of 1cm/hour (1 km / 160 000 years in prototype).

Experiments which experience high sedimentation rates (3-4 and 4-2) have a similar kinematic segmentation to those seen in low sedimentation models. The listric faults, particularly LDFs, however, are more developed in high sedimentation models (Fig. 3.9). Unlike the LDFs seen previously, these are not the result of silicone expulsion, but of high strain fault development.

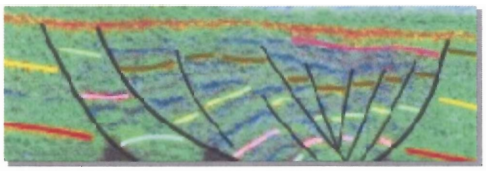

Figure 3.9: above: Detail of a cross section from experiment 3-4 showing a BDF in collapse phase, with the beginnings of a LDF (right side) with salt rollers at their base. Rollover anticline collapse structure is a keystone graben. Sediments are 5cm thick in image.

An interpretation of experiment 3-4 has been made (Fig. 3.10), showing how the cross sections and PIV data fit together. The finite (or total) strain and total subsidence show that there has been higher strain rates and more subsidence than seen in the stagnation or low sedimentation models (see Section 3.2). Both expulsion rollovers and LDF rollover systems are labelled present, as well as grabens in the shelf and BDFs in shelf and slope. The large area of silicone (black) near the end of the cross sections is a post-experimental passive diapir which pierced the post-experimental cover. Although this was not

intended, such features could result in prototypes for experiments with thick silicone layers (>2cm which is 2km in nature) if the sedimentation supply was somehow shut-off and the underlying salt was allowed to rise as passive diapirs.

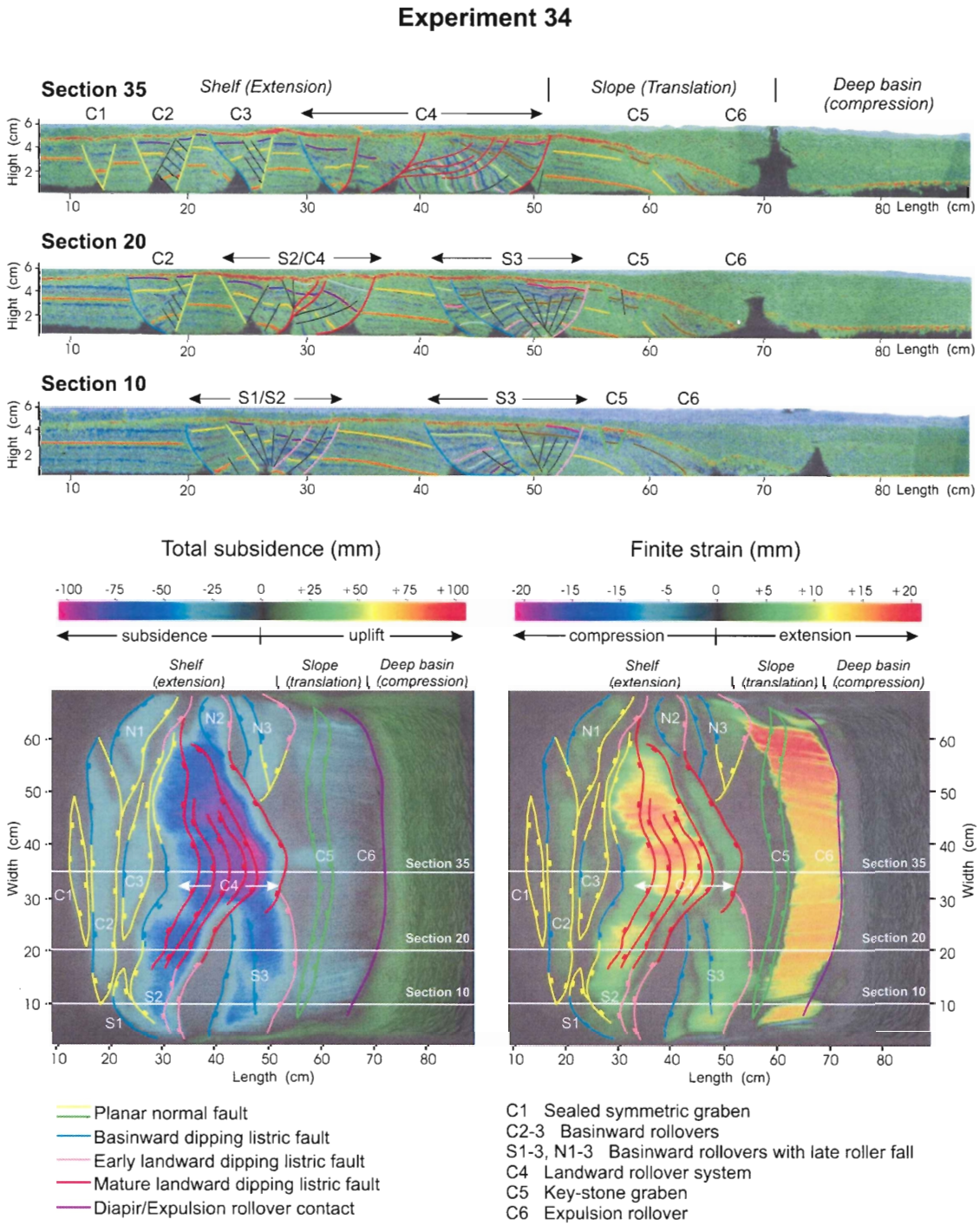

Figure 3.10: Interpretation of experiment 3-4 (high sedimentation on a flat base) showing three of the cross sections (above) and PIV data for total subsidence and total strain. (By Csaba Krezsek)

3.1.6 Progradation, and High Sedimentation Rates on a Tilted Base

Experiment 4-2, experienced the same shelf build up, slope progradation, and sedimentation rates as experiment 3-4. Its only difference is that it was conducted with its base tilted 2° and for a longer time (until the slope progradation reached the deep basin). The structures observed are similar to those seen in the flat-model counterpart (experiment 3-4). The BDFs and LDFs are well developed, with salt rollers at their base and bound by rafts welded during the late stage of the model's development at their base. The LDF rollover systems are the most developed in this model compared to the others (Fig. 3.11). Allochthonous silicone is present in the deep basin in experiment 4-2, very similar to that seen in the low sedimentation on a tilted base experiment (experiment 4-3).

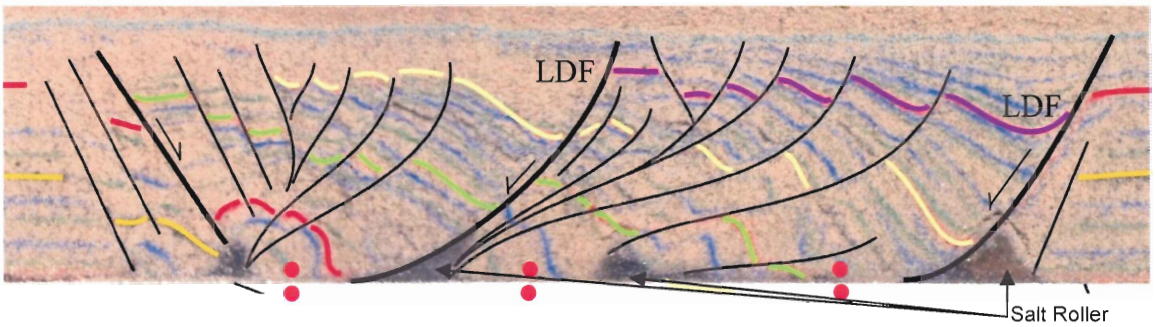

Figure 3.11: Part of a cross section from experiment 4-2 showing highly developed LDF, with associated salt rollers. Sedimentary sequence is 5cm thick.

Please see appendix I for complete cross sections.

The PIV data for experiment 4-2 (Fig. 3.12) looks very similar to that of 3-4, until later in its evolution when the large LDF seen in Figure 3.11. The subsidence shifts to the basin side of the graben, allowing for greater accommodation on the basinward side of the fault. This is evident both in the thickened strata (Fig. 3.11) and the purple coloured regions in the PIV subsidence data (Fig. 3.12).

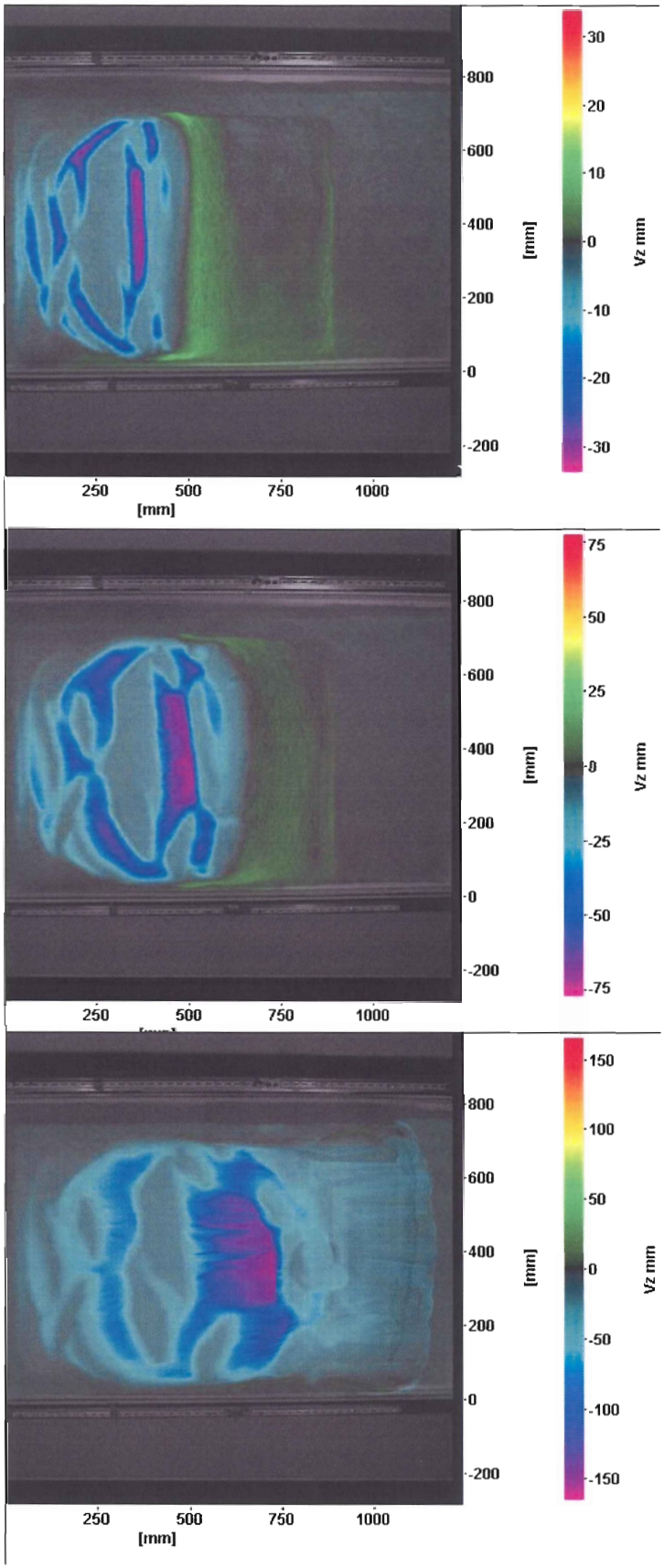

Figure 3.12: PIV data for total subsidence of experiment 4-2, from early (top), mid (middle), and late (bottom image) in its evolution. The subsidence shifts to the frontal edge of the front structure, as seen in the middle image, representing the large LDF. Note scale bar differences in each image.

3.2 Conclusions Drawn from Results

As described in Section 3.1, there are no general differences in the development of structures seen in flat base models compared to tilted base models. These models deform faster than flat base models. Thus, all of the structures seen only in tilted base models, such as the ubiquitous allochthonous silicone in the deep basins, would have also occurred in flat base models if they were conducted until the slope prograded to the basin edge of the model. Each of the experiments shows the same kinematic domains, as seen in Figure 3.13, where similar structures are observed in the domains in each experiment.

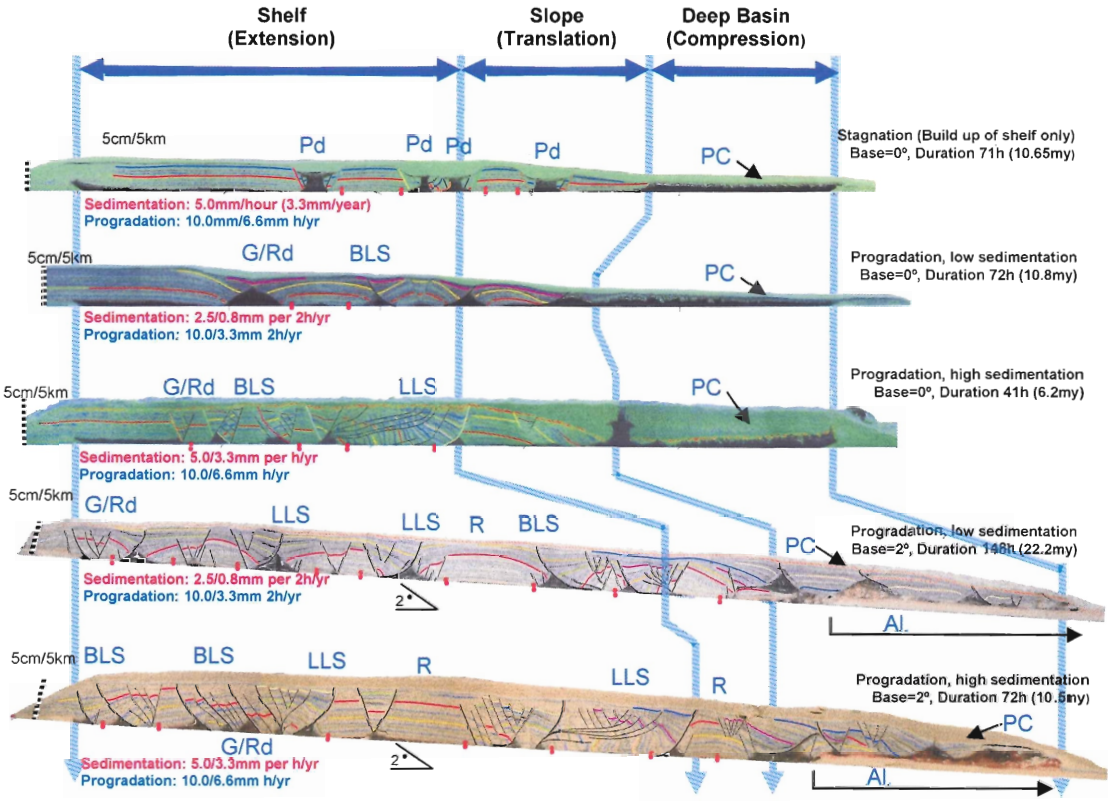

Figure 3.13: Enhanced cross sections of 5 different experiments, showing the kinematic domains. Each section is from the centre of the experiments. The black areas are silicone. Although there are different structures, the same kinematic domains (extension, translation, and compression) are in each experiment. Pd=passive diapirism; PC=post experiment cover; G/Rd=Graben systems and reactive diapirism; Pd/Ro=Passive diapirism and symmetric rollovers; R=Raft; Al.=Allochthonous silicone; Two red dots=Weld.

Taking into consideration the differences in sedimentation rates and the tilted base, it suggested here that the types of structures are strongly dependent on the strain rates. In the experiments the strain rate is directly controlled by the sedimentation pattern and rates. A sequence of structural graben evolution can be deduced from the PIV data and structural interpretations. Conjugate faults show the initial subsidence and strain localisation in symmetric graben structures followed by asymmetric grabens with basinward dipping growth fault/rollover systems and finally landward dipping growth fault/rollover systems. In the stagnation models, the strain rates are not sufficiently high enough to develop basinward or landward dipping faults because of the lack of sedimentation. In low sedimentation models, there are only minor, late stage LDF rollover systems observed, that develop from early symmetric expulsion rollovers. The models with high sedimentation rates have highly developed LDF rollover systems in addition to BDFs and sealed symmetric grabens. Figure 3.14 graphically shows how finite strain is related to time, as interpreted from the LDF rollover system seen experiment 3-4 (graben C-4 in Fig. 3.10).

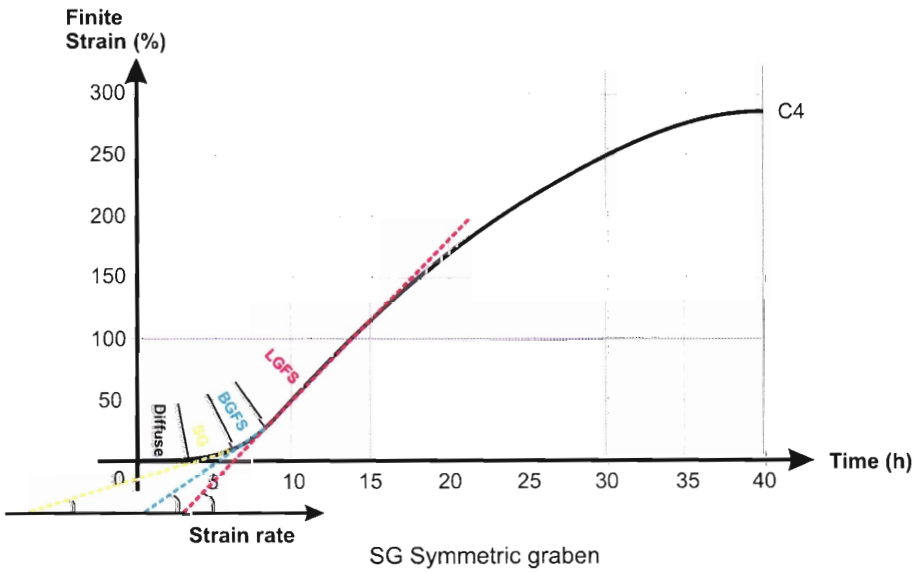

SG Symmetric graben
BGFS Basinward Growth Listric Fault/Roller System
LGFS Landward Growth Listric Fault/Roller System

Figure 3.14: Strain Rates and Finite Strain (over time) based PIV strain data in the LDF rollover system of graben C-4 of experiment 3-4. As strain rate increases, the structures evolve from symmetric grabens, to landward dipping faults (By Csaba Kreszek).

The amount of extension is also controlled by the sedimentation rates, as shown in Figure 3.15. Stagnation models experience extension earlier than other experiments, and high sedimentation experiments experience greater extension. It is also observed that the greatest extension is observed at the center of the experiments, where it is less affected by friction at the edges.

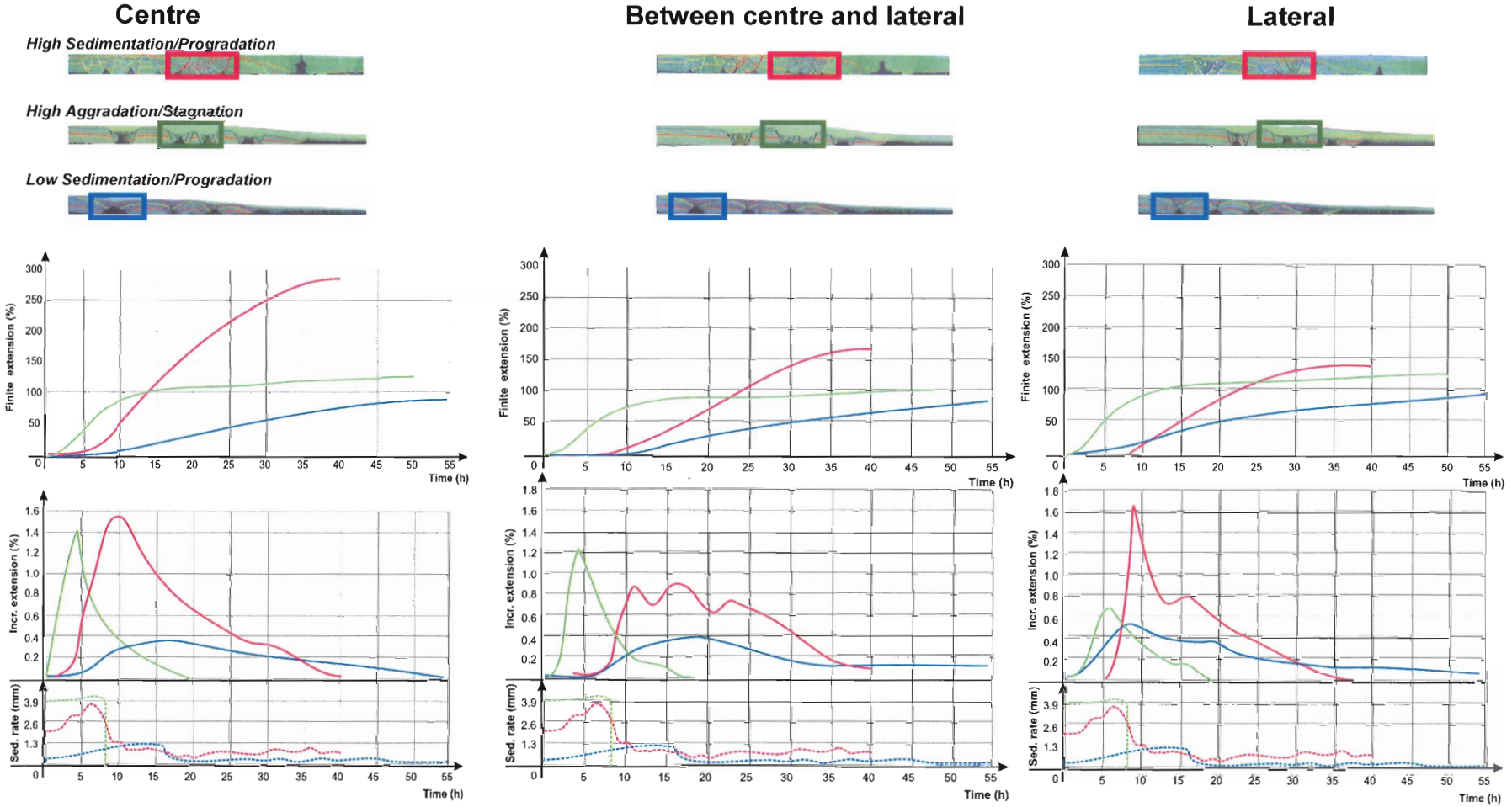

Figure 3.15: (Previous page) Comparison of finite extension (top graphs), incremental extension (middle graphs), and sedimentation rates (bottom graphs). Graphs on the left are from the centre of the experiments, the graphs on the left are from the lateral (edge) part, and the middle graphs are from the area between the centre and the lateral. Three horizontal base experiments are shown: high sedimentation (red), stagnation (green) and low sedimentation (blue). It shows that the greatest amount of extension was experienced by the high sedimentation experiments, and the stagnation models experienced extension earlier than the other experiments.

If there is not sufficient accumulated strain, the structures will not reach the LDF stage, and will stop earlier. High sedimentation rates cause faster thinning of underlying silicone which increases the ductile/brittle coupling. The evolution path of graben structures can be estimated from the sedimentation / strain rates when outer boundary conditions are constant (salt thickness basement topography) (Fig. 3.16), as seen in high sedimentation models which have few basinward dipping faults and large landward dipping faults.

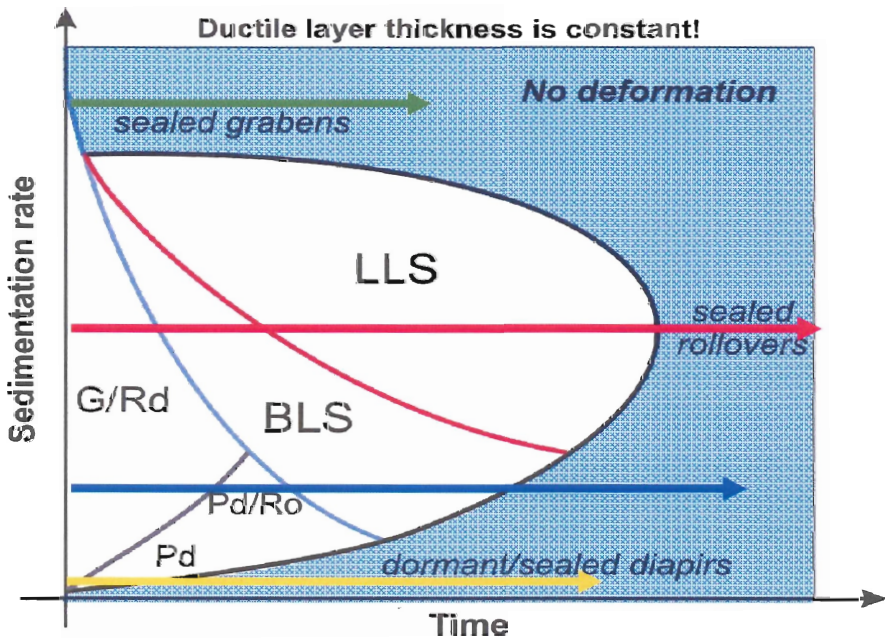

Figure 3.16: General structures developing overtime according to strain. LEGEND: BLS - Basinward listric fault/rollover systems; LLS - Landward listric fault/rollover systems; G/Rd - Graben systems and reactive diapirism; Pd - Passive diapirism; Pd/Ro - Passive diapirism and symmetric rollovers. (by Csaba Krezsek)

Figure 3.16: General structures developing overtime according to strain. LEGEND: BLS - Basinward listric fault/rollover systems; LLS - Landward listric fault/rollover systems; G/Rd - Graben systems and reactive diapirism; Pd - Passive diapirism; Pd/Ro - Passive diapirism and symmetric rollovers. (by Csaba Krezsek)

The greatest sedimentation rates are during the shelf build up. Grabens which form early, in the shelf area, are filled with sediments first. Grabens developing ahead of the prograding slope are allowed to extend before being filled by the sedimentation events when the slope reaches the structures. Thus, structures developing in the outer shelf and shelf transition area show the greatest subsidence. This is seen in experiments 3-4 (Fig. 3.10) and 4-2 (3.11 & 3.12) where large LDF rollover systems are seen in the slope/translation area and symmetric grabens are seen in the outer shelf area.

The greater extension observed in the tilted base models can be attributed to gravity. As stated in Equation 1.1, the system is stable when the forces in the shelf plus the force due to Poiseuille flow is equal to the sum of the forces in the deep basin area and the force due to Couette flow (refer to Fig. 1.4). In the horizontal experiments, gravity would be exerted on the experiment normal to the silicone. In the tilted base experiments, however, the gravity would have a vector normal to the silicone as well as a vector parallel to the silicone flow direction (Fig. 3.17). Thus, the silicone would flow towards the deep basin with out any sedimentation.

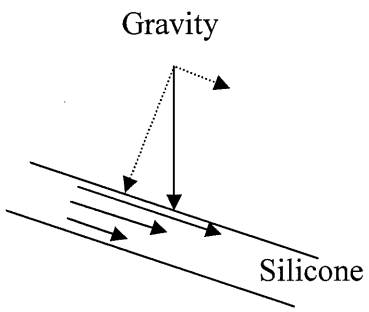

Figure 3.17: Gravity exerted on the silicone with its two components (dotted lines). Couette flow is depicted in the silicone. The gravity vector component parallel to the flow direction causes the tilted base experiment to deform sooner and extend more than experiments completed on a horizontal base.

CHAPTER FOUR: CONCLUSIONS

4.1 General Applications of Analogue Models

Analogue models improve the understanding of coupled tectonic-depositional processes. They yield information on the regional tectonic framework for structurally complex basins with mechanically constrained structural and kinematic concepts to support the interpretation of geological and geophysical data. The results of analogue models can be used to develop templates for seismic interpretation for basin analysis and petroleum system modelling. The results from the models in this thesis showed that the structures observed can be used to determine the strain rate experienced by the model. Because strain rate is determined by sedimentation patterns and rates, the depositional environment and thus the rock type can be inferred in geological settings with comparable boundary conditions. As the experiments have shown, large landward dipping rollover faults indicate high sedimentation rates (experiments 4-2 & 3-4), while slow sedimentation rates have dominantly basinward dipping roll over faults (experiments 4-3 & 3-7). Models which consist of dominantly grabens and large rafts are indicative of stagnation after aggradation of the shelf (experiments 4-1 & 3-5). Allochthonous salt tongues, such as those seen in the tilted base, suggest deformation and sedimentation processes affecting the entire area of the initial salt basin.

4.2 Application to the Scotian Margin (and Other Salt Controlled Margins)

The experiments in this thesis have some of similar structures to that seen in subsurface data from the Scotian Margin. The margin evolved by brittle-ductile deformation associated with underlying salt and sedimentary overburden sequences. In

the different salt provinces along the Scotian Margin a comparable kinematic segmentation form shelf to the deep basin (extensional, translational, and compressional domains) is proven by regional seismic studies (Shimeld, 2004). Typical salt-related structures of the margin include salt diapers, growth fault/roll over systems, grabens and sub-basins, compressional diapirs and allochthonous salt nappes in the deepwater extension, and associated stratigraphic features. Diapirs are associated with grabens above and deformed strata along their flanks (Fig 4.1). Similar features are seen in low sedimentation experiments (e.g. Fig. 3.4).

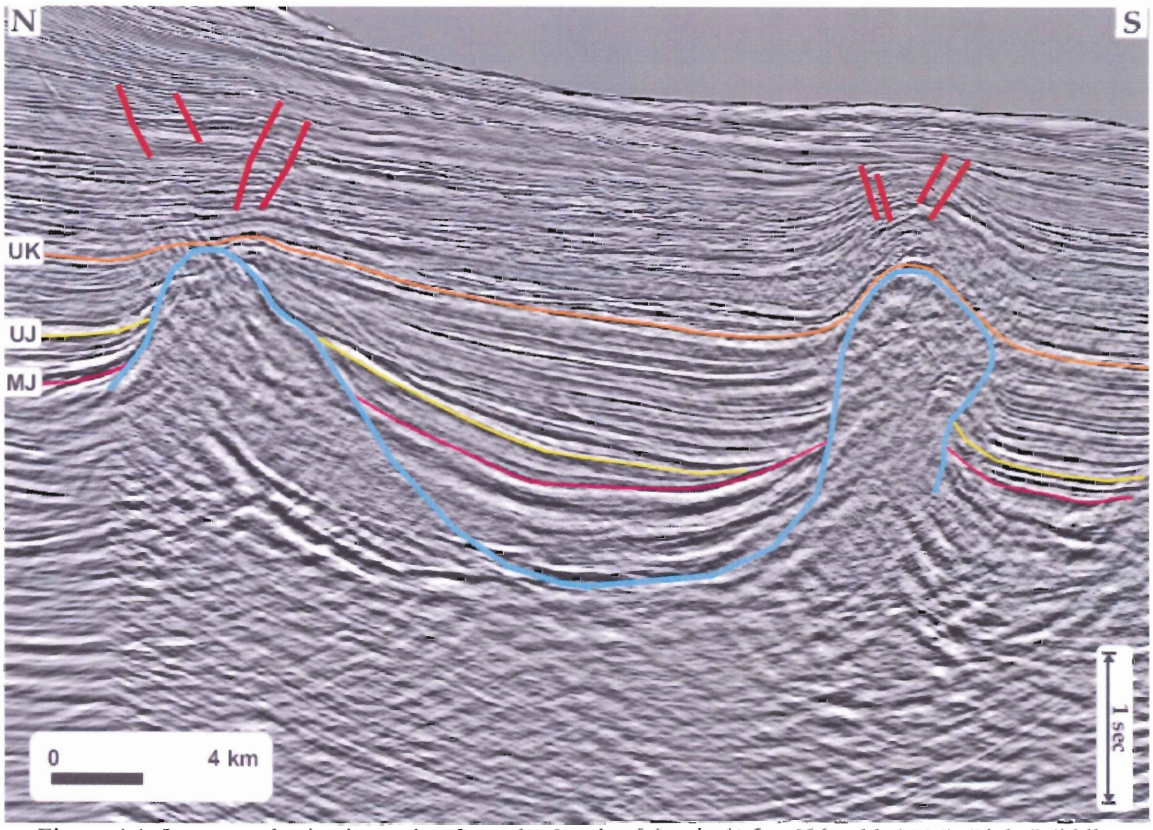

Figure 4.1: Interpreted seismic section from the Scotian Margin (After Shimeld, 2004). Pink (Middle Jurassic), yellow (Upper Jurassic) and orange (Upper Cretaceous) lines are sedimentary markers. Red marks sedimentary structures (grabens here), and blue outlines the approximate edge of the salt.

Collaboration with the Geological Survey of Canada has started to compare regional seismic data and experimental results. In the very near future (within months of this thesis being written), experiments will be developed incorporating parameters specific to the Scotian Margin sub basins. The five sub-provinces, as described by Shimeld, can be explored by addressing their individual parameters such as sedimentation rates, sediment thickness, and salt thickness. These experiments to will make direct comparisons to the margin possible:

4.3 Conclusions

Analogue experiments simulating gravity gliding of passive margin sedimentary wedges on salt substratum performed for this thesis have shown that the development of grabens and faults in brittle-ductile systems is controlled by sedimentation rates. Conversely, structures can control the paleo-environment(s) under which basin sediments were deposited. The rate at which sediments are deposited can be used to infer rock type. High sedimentation rates result in sand deposition (arenite), while slow sedimentation rates result in shale and clays (or lutite). Identification of rock type is important for interpreting the hydrocarbon potential of an area. The type of rock dictates how a given rock unit fits into the petroleum system (i.e. reservoir, seal, or migration path). Faults can act as fluid migration paths, and salt structures are impermeable to fluids such as hydrocarbons, and can act as seals. Thus, by properly interpreting the evolution of a structure identified in geological data, the development and hydrocarbon potential of a basin can be inferred.

Scaled analogue experiments give quantitative results on the deformation and depositional evolution of sedimentary basins developing on a mobile substratum, such as

salt, allowing for systematic studies on the relevant control parameters and processes. The results of the experiments are directly comparable to geological and geophysical data from natural prototypes, such as the Scotian Margin as well as data from other margins (e.g. Maudit & Brun, 1998). The experiment series in this thesis show that the structures styles are related to the strain rates experienced by the graben system, which again are controlled by the sedimentation rates. Strain rates are a function of the salt layer thickness, overburden thickness (i.e. pressure difference between shelf and basin) and the tilt of the basement. Basins with tilted basements show similar structural evolution as those on a horizontal base, but individual graben structures accumulated greater extension rates.

4.4 Future work

There remains considerable work in the use of analogue modelling and comparing it to natural prototypes such as the Scotian margin. There are at least eight fields where future work is required:

1. The reproducibility of each of the experiments should be tested by repeating the experiments using the same parameters.
2. More realistic implication of sedimentation with sequence-stratigraphy concepts.
3. Experiments with a more focused study on the influence of basement morphologies, as well as studies focusing on allochthonous salt complexes would provide more insights in basin evolution.
4. Dalhousie University has obtained a new deformation rig, which is computer controlled, allowing for more precise and consistent control and monitoring of

displacement rates, temperature, and bulk and local stresses. The primary function of this rig is to induce tectonic deformation (i.e. shortening or extending).

5. An exceptional opportunity exists at Dalhousie University to conduct studies which compare the natural, numerical, and physical experiments. Comparisons to numerical models, such as those completed by the Dalhousie Geodynamics Group, would be beneficial in furthering the understanding of brittle-ductile systems.
6. The interpreted cross sections of analogue experiments can be used for modelling of thermal evolution of a sedimentary basin. This is crucial for the understanding and prediction of thermal maturity for petroleum systems.
7. Continued investigation of the material properties of natural rocks is key to developing meaningful analogue models with appropriate materials and better scaling. This is especially true for salt because little is know about deformation mechanisms and thus about its rheology.
8. Studies on clastic rocks in nature and the properties of sands in laboratory would also be very useful. Experimental improvement would be developed through ring-shear testing of sand materials to investigate the mechanical properties of experimental sand.
9. Development of an experimental rig with automatic and precisely controlled, continuous sedimentation process. The experiments completed thus far at Dalhousie University the sedimentation events were incremental while the salt was moving continuously. A continuous sieving device may however obstruct PIV monitoring.

10. Experiments in the future could be conducted under water, as most basins exist in nature. Numerical experiments suggest that the load of water increases the stability of the slope (Gemmer, 2004). On the other hand wet sediments deform differently as the dry ones due to pore fluid pressure, and such issues with the mechanically behavior of the materials would first need to be addressed.

REFERENCES

Adam, J., Urai, J.L., Wieneke, B., Oncken, O., Pfeiffer, K., Kukowski, N., Lohrmann, J., Hoth, S., ven der Zee, W., & Schmatz, J. 2005. Shear localisation and strain distribution during tectonic faulting – new insights form granular-flow experiments and high resolution optical image correlation techniques. Journal of Structural Geology, 27: 283-301.

Bally, A.W., Bernoulli, D., Davis, G.A., & Montadert, L. 1981. Listric normal faults. Ocanologica Acta, 4: supplement: 87-101.

Byerlee, J. 1978. Friction of Rocks. Pure and Applied Geophysics, 116: 615-626.

Bucky, B.P. 1931. The use if models for the study of mining problems, Technical Publication, American Institute of Mining Engineers, 425.

Burollet, P.F. 1975. Tectonique en radeau en Angola. Bulletin of Geological Society of France, 17: 503-504.

Cadell, H.M. 1887. Experimental Researched in Mountain Building. Royal Society of Edinburgh Transactions, 35: 337-360.

Cobbold, P.R. 2001. Information Sheets about Silicone Putty. (05/28/2004). **<www.es.usyd.edu.au/geology/people/staff/prey/Que...>**

Cobbold, P.R. & Jackson, M.P.A. 1992. Gum Rosin (colophony): a suitable material for themomechanical modelling of the lithosphere. Tectonics, 210: 255-271.

Costa, E. & Vendeville, B.C. 2002. Experimental insights on the geometry and kinetics of fold-and-thrust belts above weak, viscous evaporitic decollement. Journal of Structural Geology, 24: 1729-1739.

Daubre, A. 1979. Etudes synthétiques de géologie expérimentale. Dunod, Paris.

Favre, A. 1978. Archives des Sciences Physique et Naturelles, 246.

Fort, X., Brun, J.-P. , Chauvel, F. 2004. Kinematics and dynamics of salt tectonics driven by progradation. AAPG Bulletin 88: 1523–1544.

Gemmer, L., Ings, S.J., Medvedev, S., & Beaumont, C. 2004. Salt tectonics driven by differential sediment loading: Stability analysis and finite-element experiments. Basin Research, 16: 199-218.

Gibbs, A.D. 1984. Structural evolution of extensional basin margins. Journal of the

Geological Society of London, 141:4: 609-620.

Grujic, D. In Press. Channel flow and continental collision tectonics: an overview. In: Law, R.D., Searle, M.P., & Goodin, L. (eds.) Channel Flow, Extrusion, and Exhumation in Continental Collision Zones. Geological Society, London, Special Publications.

Grujic, D., Walter, T.R., & Gaertner, H. 2002. Shape and structure of (analogue models of) refolded layers. Journal of Structural Geology, 24:8: 1313-1326.

Hall, J. 1815. On the vertical position and convolution of certain strata and their relation with granite. Royal Society of Edinburgh Transactions, 7: 79-108.

Hubbert, M.K. 1937. Theory of scale models as applied to the study of geological structures. Geological Society of America Bulletin, 48: 1459-1520.

Hubbert, M.K. 1951. Mechanical basis for certain familiar geological structures. Geological Society of America Bulletin, 62: 355-372.

Imber, J., Childs, C., Nell, P.A.R., Walsh, J.J., Hodgetts, D., & Flint, S. 2003. Hanging wall fault kinematics and footwall collapse in listric growth fault systems. Journal of Structural Geology, 25:2: 197-208.

Jackson, M.P.A. , & Talbot, C.J. 1994. Advances in salt tectonics. Pergamon Press: Tarrytown: New York. 159-179.

Jackson, M.P.A., & Vendeville, B.C. 1992. Initiation of diapirism by regional extension; geological society of america, 1992 annual meeting, Abstracts with Programs - Geological Society of America, 24: 279-280.

Jaeger, J.C. & Coo, N.G.W. 1976. Fundamentals of rock mechanics. Wiley: New York, 585 pp.

Kidston, A.G., Brown, D.E., Altheim, B., Smith, B.M. 2002. Hydrocarbon potential of the deep-water Scotian Slope. Canada-Nova Scotia Offshore Petroleum Board. (09/10/2005) <www.cnsopb.ns.ca/archives/pdf/Hydrocarbon_Potential_Scotian_Slope.pdf>

Koyi, H. 1997. Analogue modelling: From a qualitative to a quantitative technique – A historical outline. Journal of Petroleum Geology, 20: 223-238.

Lehner, F.K., 2000. Approximate theory of substratum creep and associated overburden deformation in the salt basins and deltas. In: Lehner, F.K. & Urai, J.L. (eds) Aspects of tectonic faulting. Springer: Berlin.

Lohrmann, J., Kukowski, N., Adam, J., & Oncken, O. 2003. The impact of analogue material properties on the geometry, kinematics, and dynamics of convergent sand wedges. Journal of Structural Geology, 10: 1-21.

Mart, Y. and Ross, D.A. 1987. Post-Miocene rifting and diapirism in the northern Red Sea. Marine Geology, 74: 3-4: 173-190.

Mauduit, T. & Brun, J.-P. 1998. Growth fault/rollover systems; birth, growth, and decay. Journal of Geophysical Research, B, Solid Earth and Planets, 103:8: 119-136.

Mc Clay, K.R. 1990. Extensional fault systems in sedimentary basins; a review of analogue model studies. Marine and Petroleum Geology, 7:3: 206-233.

McClay K.R. & Ellis, P.G. 1987. Geometries of extension fault systems developed in model experiments. Geology (Boulder), 15:4: 341-344.

Nieuwland, D.A., Urai, J.L. & Knoop, M. 2000. In-situ stress measurements in model experiments of tectonic faulting. In: Lehner, F.K. & Urai, J.L. (eds) Aspects of tectonic faulting. Springer: Berlin.

Richard, P.D., Ballard, J.F., Colletta, B. & Cobbold, P.R. 1989. Falut initiation and development above a basement strike-slip fault: analogue modelling and tomography. Compte Rendu Academie des Sciences, 309: 2111-2118.

Roberts, A. & Yielding, G. 1994. Continental extensional tectonics. In: Continental Deformation. Hancock, P.L. (ed.) Pergamon Press: Terrytown, NY. 233-250.

Römer, M. and Neugebauer, H., 1991. The salt dome problem: a multilayered approach. *J. Geophys. Res.*, **96**, 2389–2396.

Schardt, H. 1884. Geological Studies in the Pays-D'Enhant Vaudios. Bulletin de le Society Vaudois des Science Natural, 20: 143-146.

Schellart, W.P. 2002. Analogue modelling of large-scale tectonic processes: an introduction. Journal of the Virtual Explorer: 7: 1-6.

Schreurs, G., Haenni, R., Panien, M., & Vock, P. 2003. Analysis of analogue models by helical X-ray computed tomography. Geological Society Special Publications. 215: 213-223.

Shimeld, J. 2004. A comparison of salt tectonic subprovinces beneath the Scotian Slope and Laurentian Fan; Geological Survey of Canada, Contribution no. 2004025.

Turcotte, D.L., & Schubert, G. 2002. Geodynamics. Cambridge University Press:

Cambridge. 456 pp.

Twiss R.J., & Moores, M.M. 1992. Structural Geology. W.H. Freeman and Company: New York. 532 pp.

Vendeville, B.C. 2005. Salt tectonics driven by sediment progradation: Part I: Mechanics and kinematics. AAPG Bulletin. 89: 1071–1079.

Vendeville, B.C. and Jackson M.P.A. 1990. Physical modeling of the growth of extensional and contractional salt tongues on continental slopes. AAPG Bulletin 74: 784.

Vendeville, B.C. and Jackson M.P.A. 1992a. The rise of salt diapers during thin-skinned extension. Marine and Petroleum Geology, 9:4: 331-353.

Vendeville, B.C. and Jackson M.P.A. 1992b. The fall of diapirs during thin-skinned extension. Marine and Petroleum Geology, 9:4: 354-371.

Vendeville, B.C. Jackson, M. P. A., Sattar, A., Anonymous, 1994. Annual Meeting Abstracts – American Association of Petroleum Geologists and Society of Economic Paleontologists and Mineralogists 1994, 276.

Wade, J.A. and MacLean, B.C. 1990. The geology of the southeastern margin of Canada, Chapter 5 in Geology of the Continental Margin of Eastern Canada, M.J. Keen and G.L. Williams (ed.); Geological Survey of Canada, Geology of Canada, 2: 167-238.

Weijermars, R. 1986. Flow behaviour and physical chemistry of bouncing putties and related polymers in view of tectonic laboratory applications. Tectonophysics, 124:3-4: 279-286.

Willis, B. 1893. The mechanics of Appalachian structure. Unites States Geological Survey Annual Report, 13:2: 211-281.

Wosnitza, E.M., Grujic, D., Hoffmann, R., & Behrmann, J.H. 2001. New Apparatus for thermomechanical analogue modeling. Memoir – Geological Society of America. 193: 245-251.

APPENDIX I: CROSS SECTIONS

Appendix I contains the cross sections for the experiments completed in this. All are included here, except for experiment 4-1. Because some features are difficult to see at this resolution, Appendix I has been put onto CD with the cross sections in JPG format.

APPENDIX II: PIV DATA

Due to the volume of PIV data, Appendix II is found on the attached CD. It contains the PIV data, in jpg format, for all of the experiments discussed in this thesis (except 4-1).

Abbreviations used in file names:

60min:	The time difference from one image to the next is 60 minutes.
incr:	incremental (active)
sum:	total (finite)
vl:	vector length displacement
vx:	vector length in x-direction (horizontal displacement)
vz:	vector length in z-direction (vertical displacement, subsidence)
exx:	horizontal strain
vec_vl:	total deformation shown as deformed vector grid map

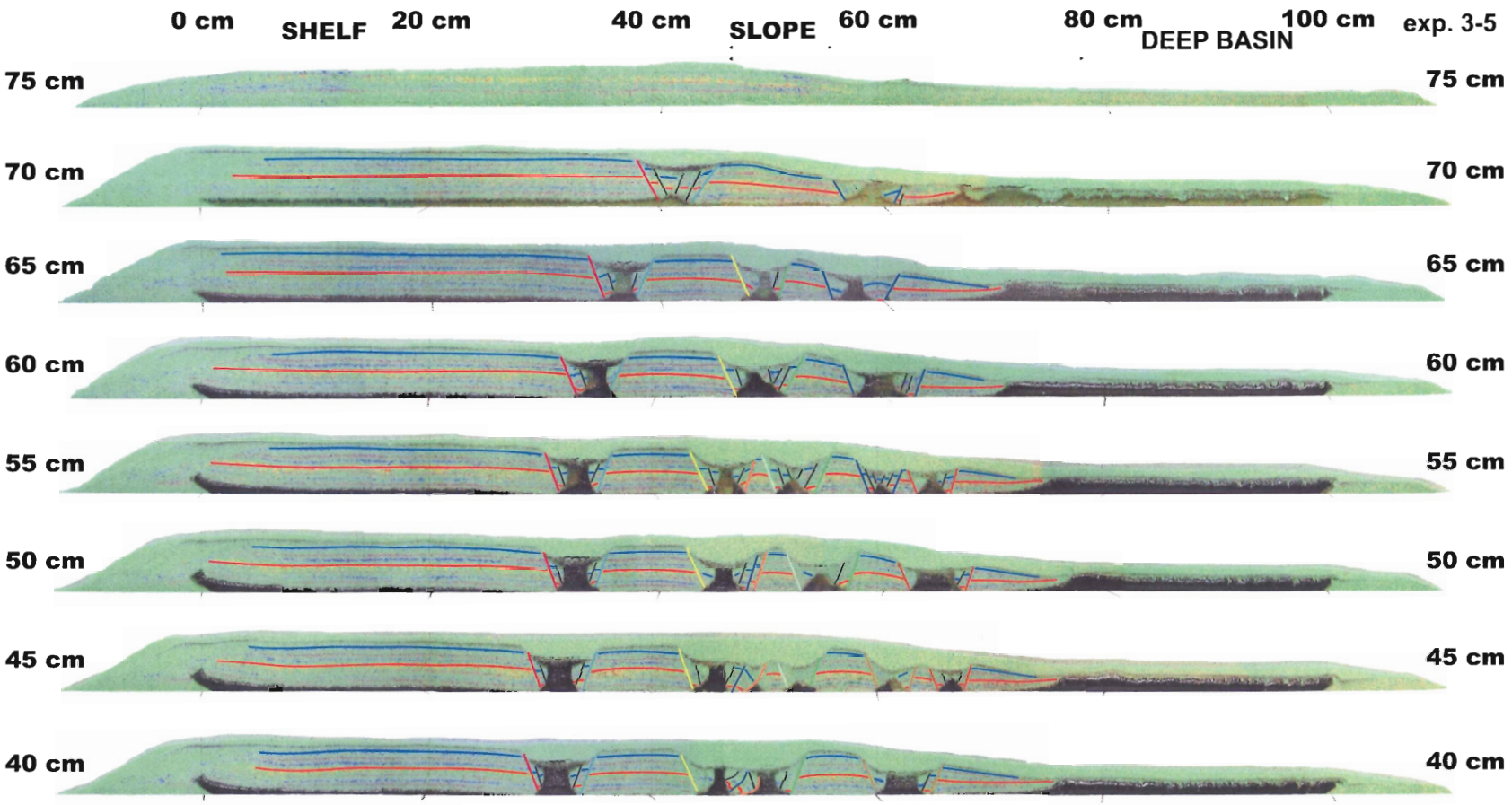
0 cm
SHELF
20 cm
40 cm
SLOPE
60 cm
80 cm
DEEP BASIN
100 cm
exp. 3-5
75 cm
70 cm
65 cm
60 cm
55 cm
50 cm
45 cm
40 cm

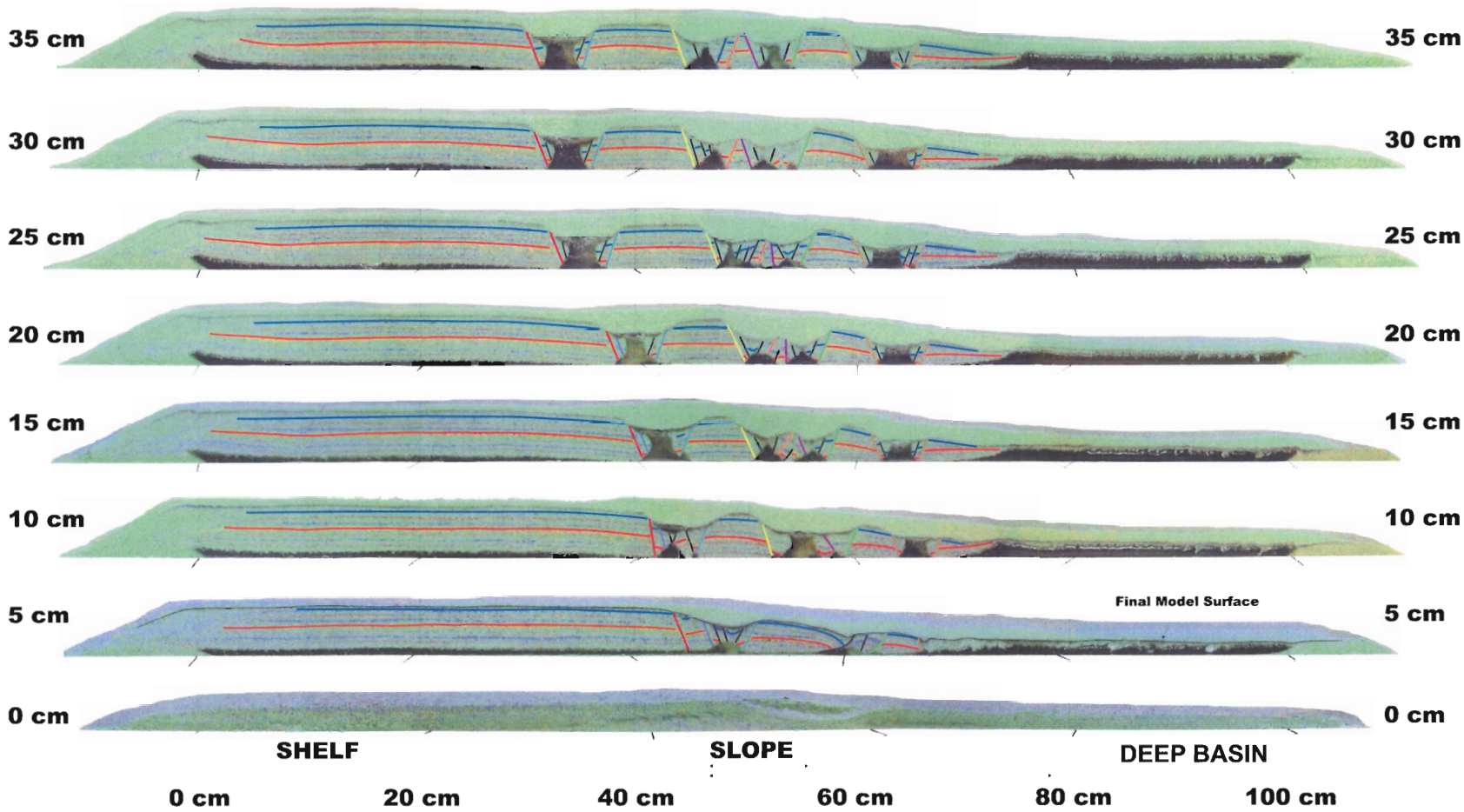

EXPERIMENT 3-5: Aggradation with Stagnation
Digitally enhanced cross section

(Interpreted by C. Krezsek)

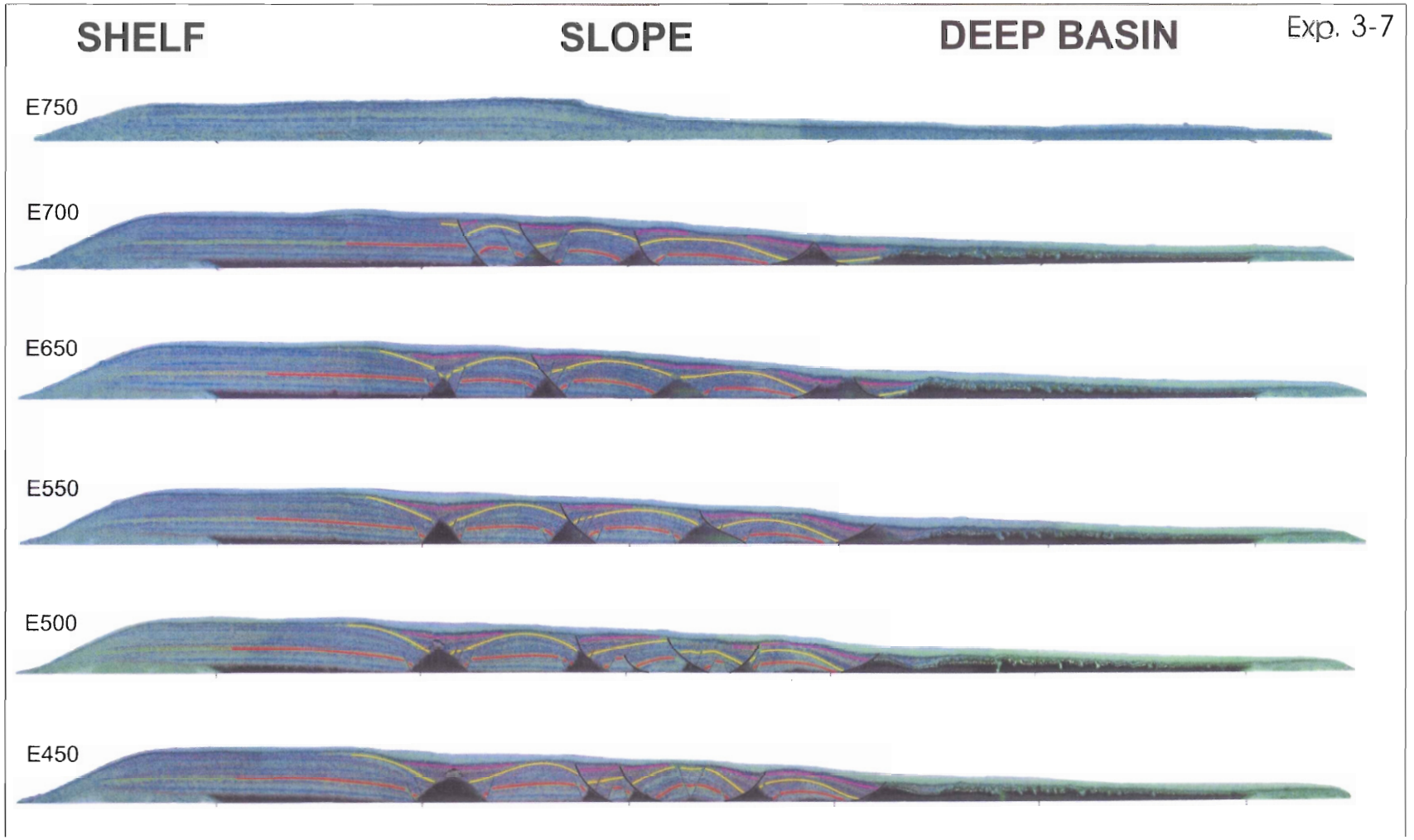
SHELF
SLOPE
DEEP BASIN
Exp. 3-7
E750
E700
E650
E550
E500
E450

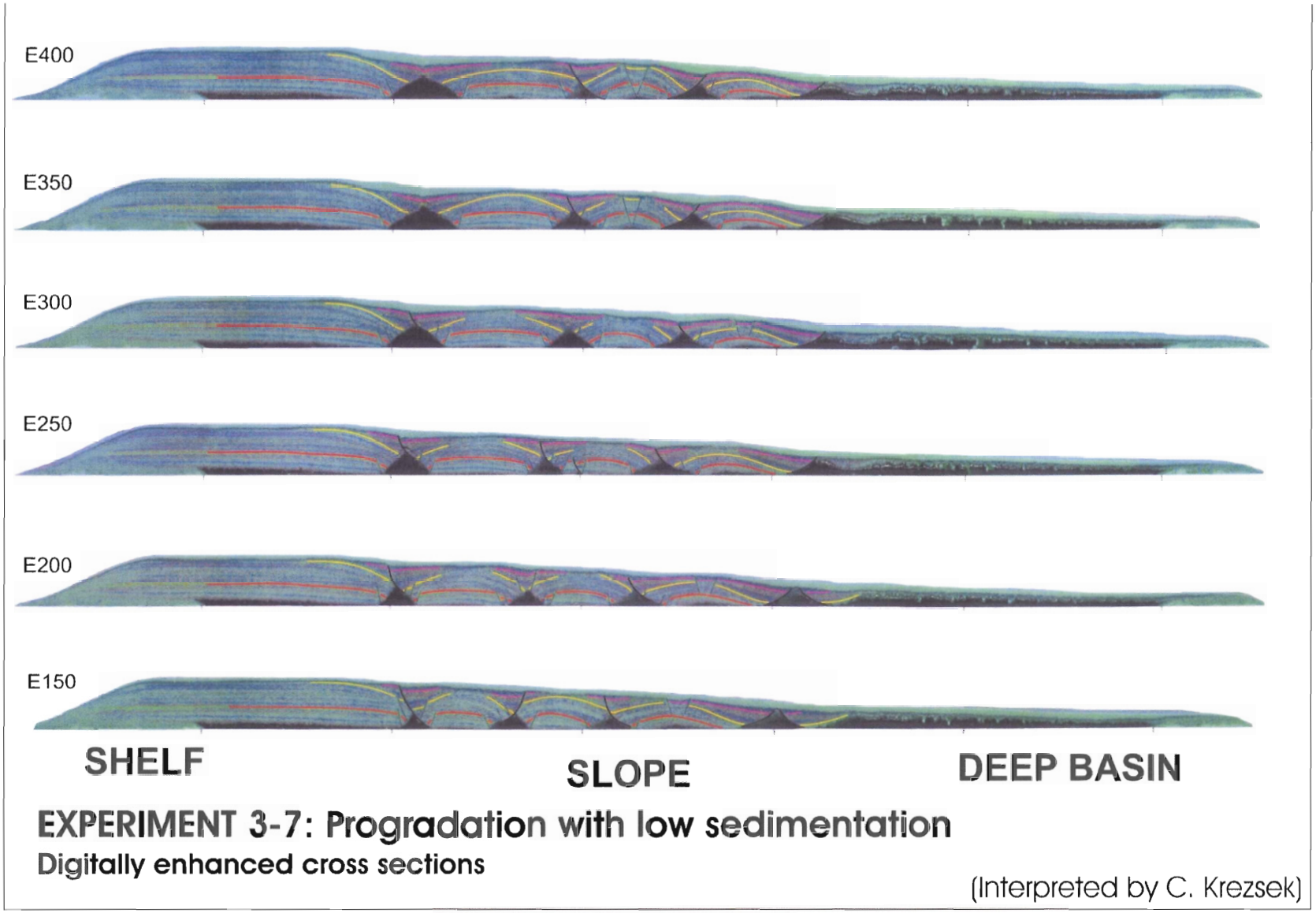

EXPERIMENT 3-7: Progradation with low sedimentation

Digitally enhanced cross sections

(Interpreted by C. Krezsek)

Appendix I

exp.3-4

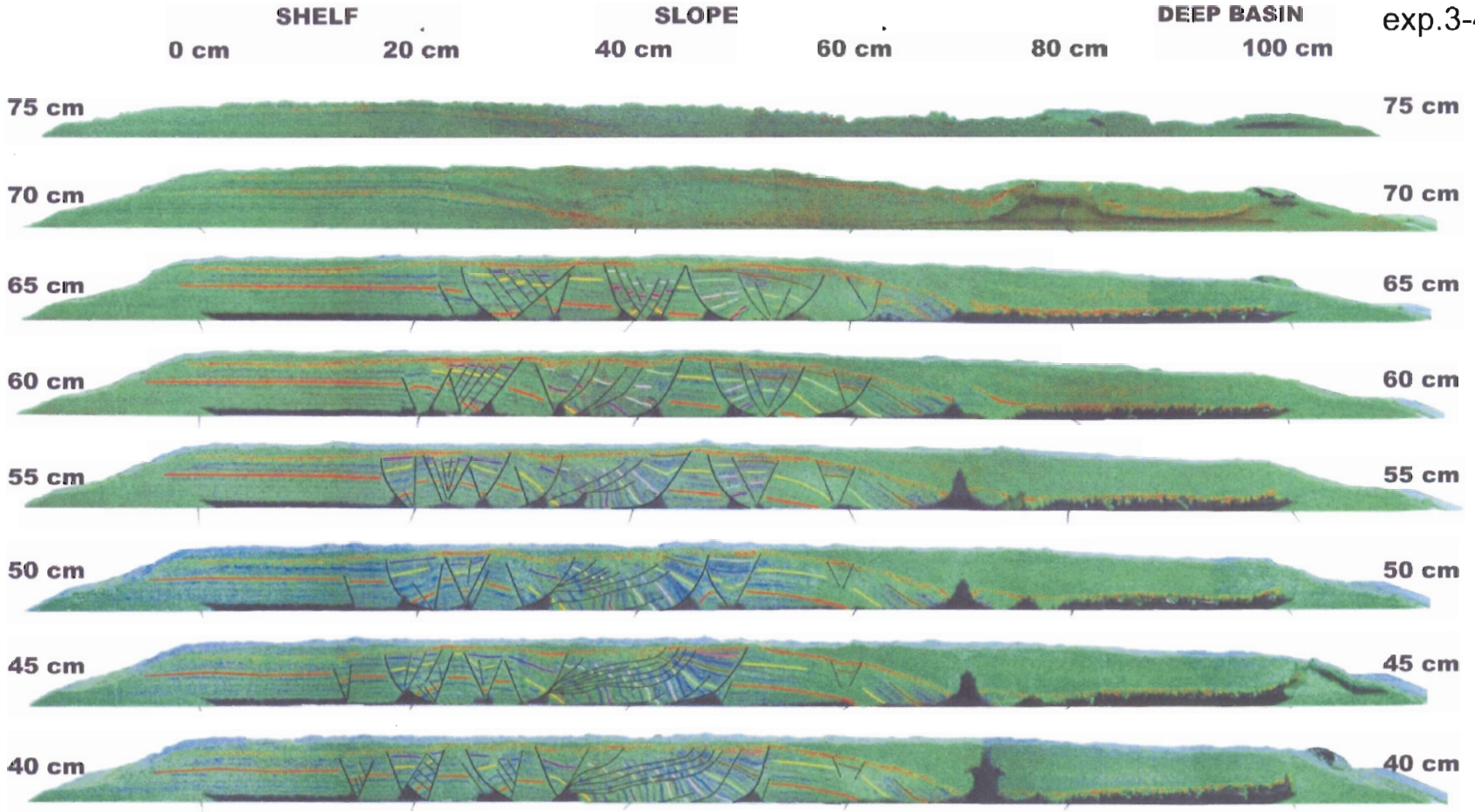

Appendix I

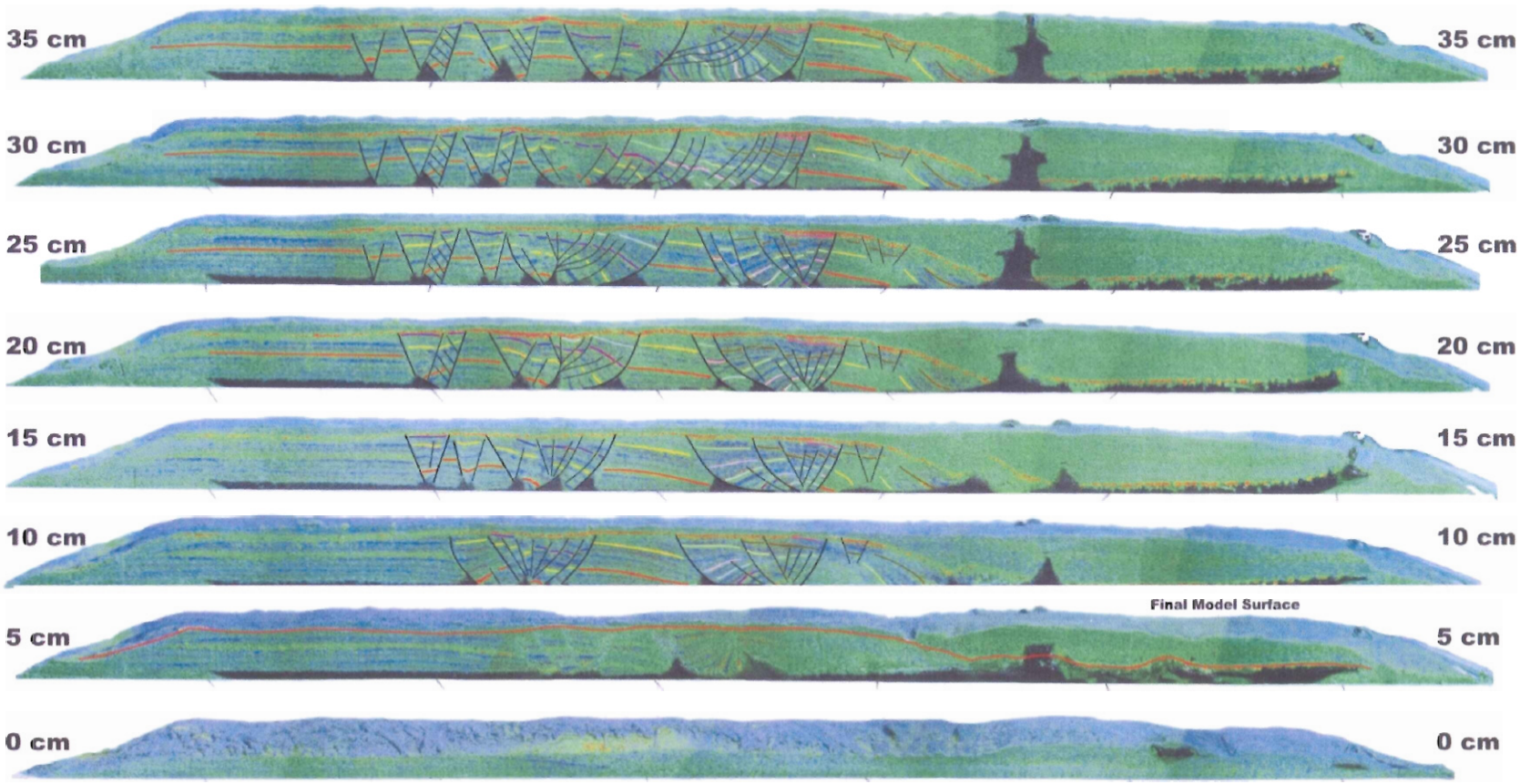

EXPERIMENT 3-4: Progradation with Sedimentation

Digitally enhanced cross sections

(Interpreted by: C. Krezsek)

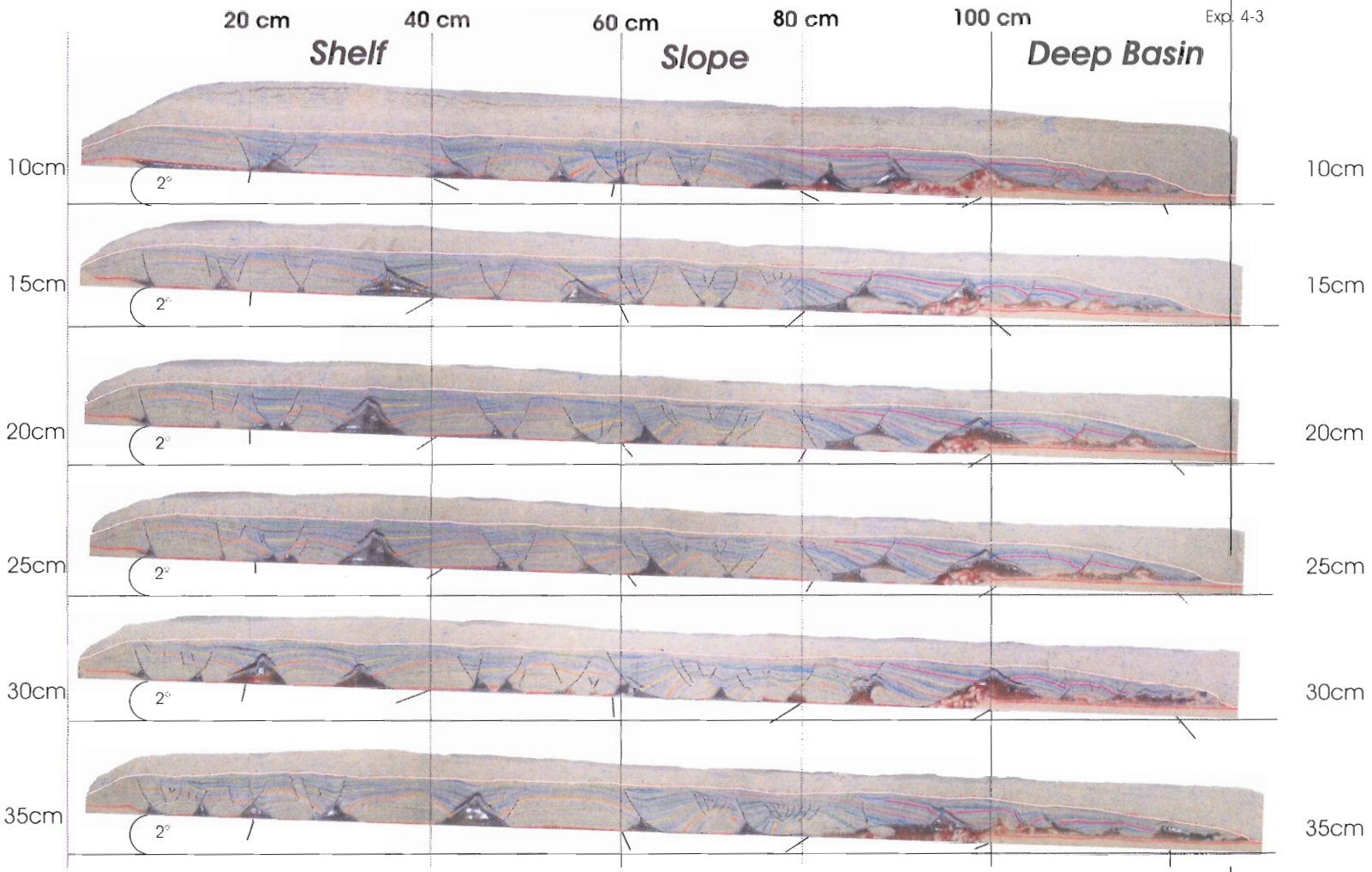
20 cm
40 cm
60 cm
80 cm
100 cm
Exp. 4-3
Shelf
Slope
Deep Basin
10cm
15cm
20cm
25cm
30cm
35cm
2°

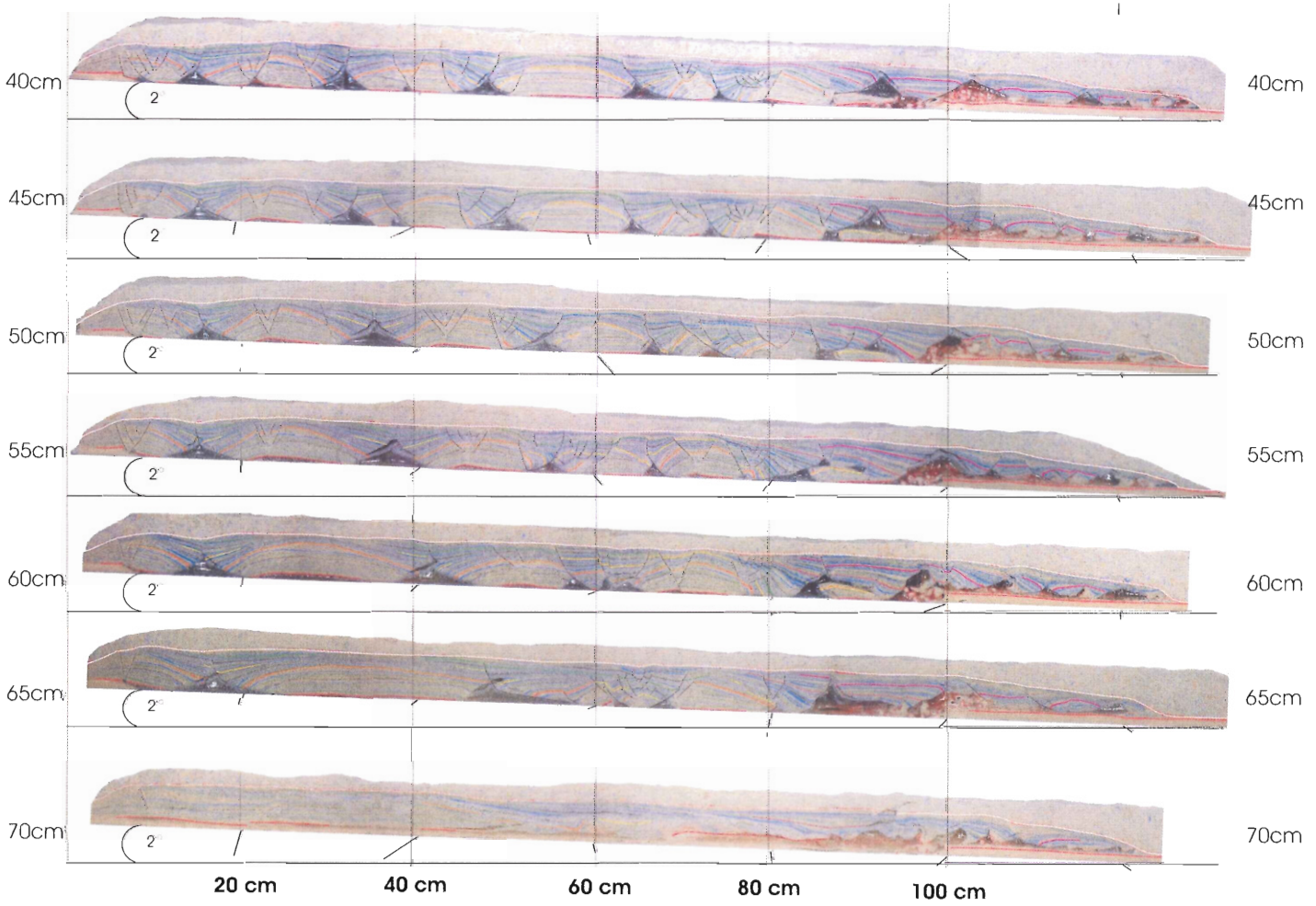

EXPERIMENT 4-3: Progradation with low sedimentation
Digitally enhanced cross sections

(Interpreted by S. Ballantyne)

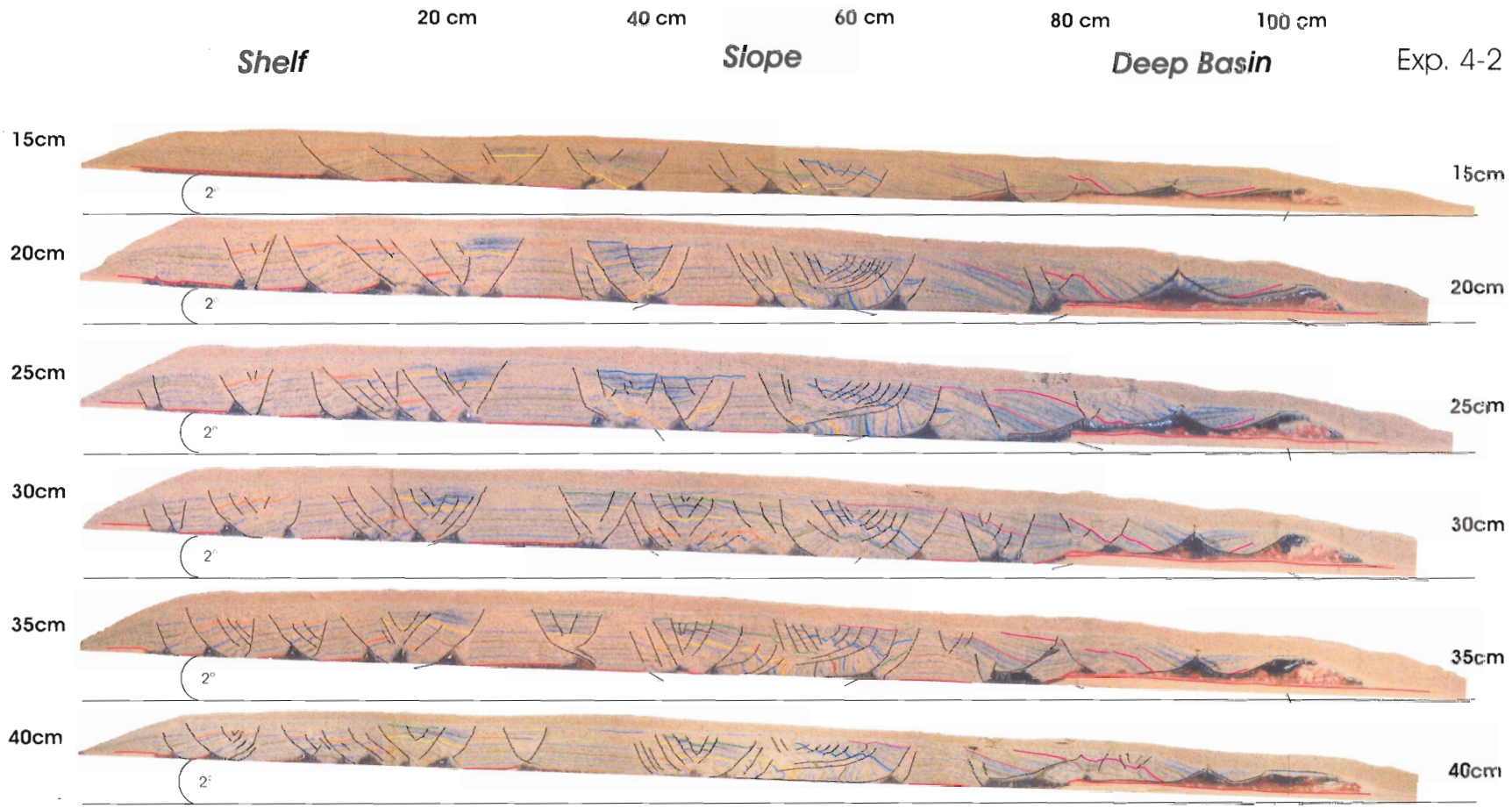
20 cm
40 cm
60 cm
80 cm
100 cm
Shelf
Slope
Deep Basin
Exp. 4-2
15cm
20cm
25cm
30cm
35cm
40cm
2°

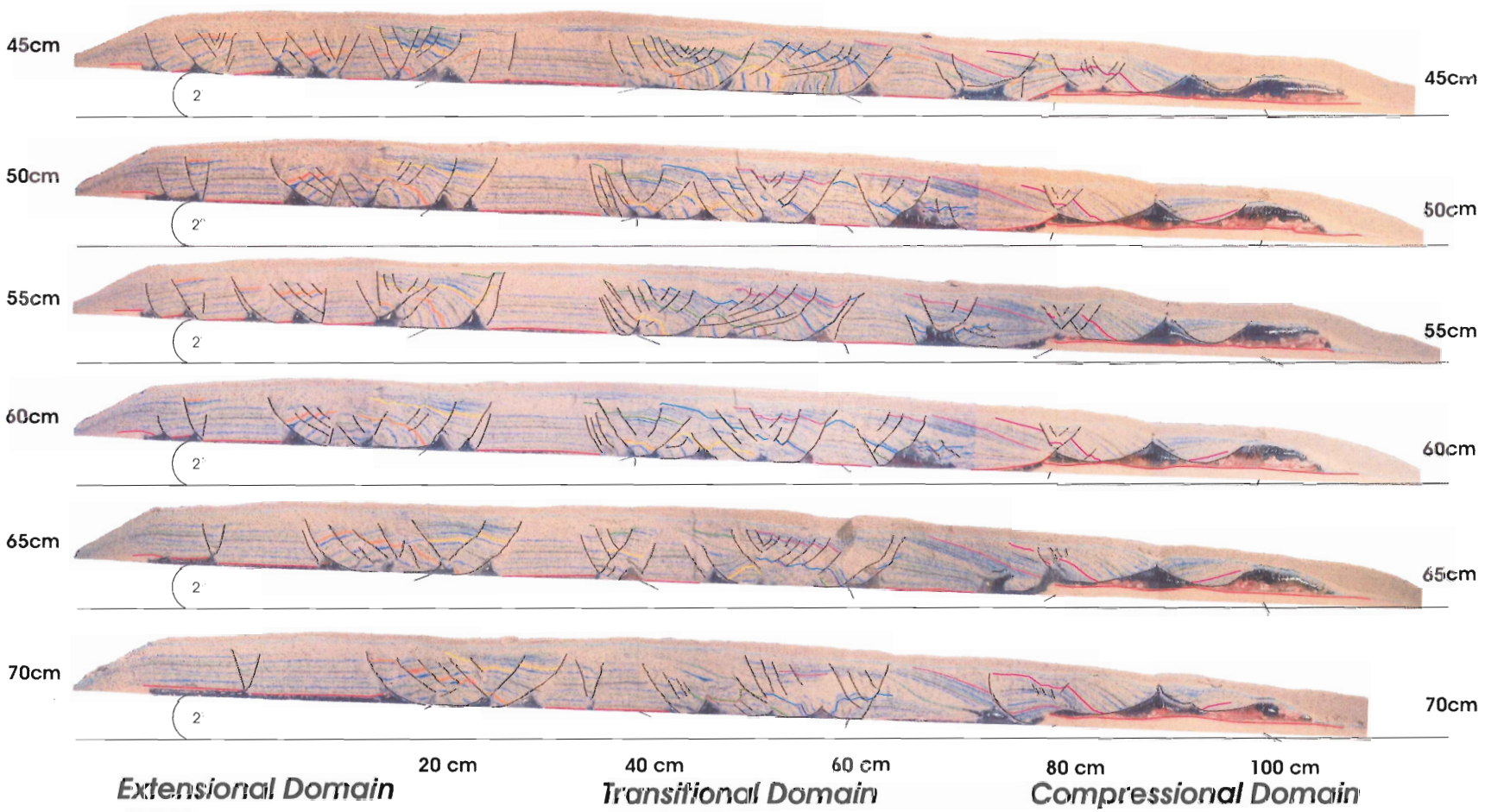

EXPERIMENT 4-2: Progradation with Sedimentation
Digitally enhanced cross sections

(Interpretted by S. Ballantyne)